

1 **Tracing genetic exchange and biogeography of *Cryptococcus neoformans* var.**
2 ***grubii* at the global population level**

3 Johanna Rhodes^{1*}, Christopher A. Desjardins^{2*}, Sean M. Sykes², Mathew A. Beale^{1,3,4},
4 Mathieu Vanhove¹, Sharadha Sakthikumar², Yuan Chen⁵, Sharvari Gujja², Sakina Saif²,
5 Anuradha Chowdhary⁶, Daniel John Lawson⁷, Vinicius Ponzio⁸, Arnaldo Lopes Colombo⁸,
6 Wieland Meyer^{9,10}, David M. Engelthaler¹¹, Ferry Hagen^{12,13}, Maria Teresa Illnait-Zaragozi¹⁴,
7 Alexandre Alanio¹⁵, Jo-Marie Vreulink¹⁶, Joseph Heitman¹⁷, John R. Perfect⁵, Anastasia
8 Litvintseva¹⁷, Tihana Bicanic³, Thomas S. Harrison³, Matthew C. Fisher^{1#}, Christina A.
9 Cuomo^{2#}

10 1 - Department of Infectious Disease Epidemiology, Imperial College London, London, W2
11 1PG United Kingdom

12 2 - Broad Institute of MIT and Harvard, Cambridge, Massachusetts 02142, USA

13 3 - Institute of Infection and Immunity, St. George's University London, London WC1E 6BT,
14 United Kingdom

15 4- Wellcome Trust Sanger Institute, Wellcome Genome Campus, Cambridge, United
16 Kingdom

17 5 - Division of Infectious Diseases, Department of Medicine, Duke University Medical Center,
18 Durham, North Carolina 27710, USA

19 6 - Department of Medical Mycology, Vallabhbhai Patel Chest Institute, University of Delhi,
20 Delhi 110007, India

21 7 - Integrative Epidemiology Unit, School of Social and Community Medicine, University of
22 Bristol, Bristol BS8 1TH, United Kingdom

23 8 – Division of Infectious Diseases of the Federal University of São Paulo-UNIFESP, São
24 Paulo 04039-032, Brazil

25 9 - Molecular Mycology Research Laboratory, Centre for Infectious Diseases and
26 Microbiology, Sydney Medical School-Westmead Hospital, Marie Bashir Institute for
27 Infectious Diseases and Biosecurity, The University of Sydney, Westmead Institute for
28 Medical Research, Sydney, Australia

29 10 - Mycology Laboratory, Evandro Chagas National Institute of Infectious Diseases,
30 Oswaldo Cruz Foundation, Rio de Janeiro, Brazil

31 11 - TGen North, Translational Genomics Research Institute, Flagstaff, Arizona, USA

32 12 - Department of Medical Microbiology and Infectious Diseases, Canisius-Wilhelmina
33 Hospital, Nijmegen, The Netherlands

34 13 - Centre of Expertise in Mycology Radboudumc/CWZ, Nijmegen, the Netherlands

35 14 - Departamento Bacteriología-Micología, Centro de Investigación, Diagnóstico y
36 Referencia, Instituto de Medicina Tropical Pedro Kourí La Habana, Cuba

37 15 - Laboratoire de Parasitologie-Mycologie, AP-HP, Groupe Hospitalier Saint-Louis-
38 Lariboisière-Fernand-Widal Paris, France; Université Paris Diderot, Sorbonne Paris Cité,
39 Paris, France; Unité de Mycologie Moléculaire, Institut Pasteur, Centre National de la
40 Recherche Scientifique, Centre National de Référence Mycoses Invasives et Antifongiques,
41 URA3012 Paris, France.

42 16 - Department of Microbiology, Stellenbosch University, Stellenbosch, South Africa

43 17 - Department of Molecular Genetics and Microbiology, Duke University Medical Center,
44 Durham, North Carolina, USA

45

46 *These authors contributed equally to this work

47

48 # Corresponding authors

49 All sequence data from this study have been submitted to GenBank under BioProject ID
50 PRJNA 384983 (<http://www.ncbi.nlm.nih.gov/bioproject>).

51

52 Running title: *Cryptococcus* global population genomics.

53

54 Keywords: *Cryptococcus*; hybridization; phylogeography; recombination; selection; genome
55 sequence.

56

57 Corresponding authors: Christina A. Cuomo, Broad Institute, Cambridge MA 02142 USA.
58 Phone: 617-714-7904. Email: cuomo@broadinstitute.org. Matthew C. Fisher, Imperial
59 College London, London, W2 1PG United Kingdom. Phone: +44 (0) 20 7589 5111. Email:
60 matthew.fisher@imperial.ac.uk.

61

62

63 **Abstract**

64 *Cryptococcus neoformans* var. *grubii* is the causative agent of cryptococcal meningitis, a
65 significant source of mortality in immunocompromised individuals, typically HIV/AIDS
66 patients from developing countries. Despite the worldwide emergence of this ubiquitous
67 infection, little is known about the global molecular epidemiology of this fungal pathogen.
68 Here we sequence the genomes of 188 diverse isolates and characterized the major
69 subdivisions, their relative diversity and the level of genetic exchange between them. While
70 most isolates of *C. neoformans* var. *grubii* belong to one of three major lineages (VNI, VNII,
71 and VNB), some haploid isolates show hybrid ancestry including some that appear to have
72 recently interbred, based on the detection of large blocks of each ancestry across each
73 chromosome. Many isolates display evidence of aneuploidy, which was detected for all
74 chromosomes. In diploid isolates of *C. neoformans* var. *grubii* (serotype A/A) and of hybrids
75 with *C. neoformans* var. *neoformans* (serotype A/D) such aneuploidies have resulted in loss
76 of heterozygosity, where a chromosomal region is represented by the genotype of only one
77 parental isolate. Phylogenetic and population genomic analyses of isolates from Brazil
78 reveal that the previously 'African' VNB lineage occurs naturally in the South American
79 environment. This suggests migration of the VNB lineage between Africa and South America
80 prior to its diversification, supported by finding ancestral recombination events between
81 isolates from different lineages and regions. The results provide evidence of substantial
82 population structure, with all lineages showing multi-continental distributions demonstrating
83 the highly dispersive nature of this pathogen.

84

85 Introduction

86 The environmental basidiomycetous yeast *Cryptococcus neoformans* is capable of causing
87 invasive fungal infections primarily in immunocompromised individuals. Meningitis is the
88 most serious manifestation of cryptococcosis. The HIV/AIDS pandemic increased the
89 population of these susceptible individuals and led to an increase in *C. neoformans* infection
90 rates (Day, 2004). *C. neoformans* is the leading cause of mortality in HIV/AIDS patients
91 worldwide, particularly in sub-Saharan Africa, where approximately half a million deaths
92 occur annually (Park et al., 2009). While cryptococcal infection rates in HIV positive
93 individuals have declined due to highly active antiretroviral therapy (HAART), new estimates
94 continue to suggest there are more than 100,000 deaths/year (Rajasingham et al., 2017);
95 recent data also suggests that the incidence of cryptococcosis has plateaued at a high
96 number despite HAART availability. Furthermore, the increasing number of people living with
97 other immunodeficiencies, including transplant and cancer patients, represents a growing
98 population at risk for cryptococcosis (Maziarz and Perfect, 2016).

99 There are three major serotypes of *Cryptococcus neoformans* distinguished by different
100 capsular antigens, which include two separate varieties (*Cryptococcus neoformans* var.
101 *grubii* and *Cryptococcus neoformans* var. *neoformans*, serotypes A and D respectively) and
102 a hybrid between the two (serotype AD). While *C. neoformans* isolates are primarily haploid,
103 diploid AD hybrid isolates consisting of both serotype A (*C. neoformans* var. *grubii*) and
104 serotype D (*C. neoformans* var. *neoformans*) have been isolated from both clinical and
105 environmental sources mostly in Europe (Cogliati, 2013; Desnos-Ollivier et al., 2015;
106 Franzot et al., 1999). Serotype A isolates are the most common cause of infection,
107 accounting for 95% of all *C. neoformans* infections globally (Casadevall and Perfect, 1998;
108 Heitman et al., 2011). Genomes of serotype A and D isolates differ by 10-15% at the
109 nucleotide level (Janbon et al., 2014; Kavanaugh et al., 2006; Loftus et al., 2005), and
110 laboratory crosses of A and D isolates are possible but show reduced viability of meiotic
111 spores (Lengeler et al., 2001; Vogan and Xu, 2014).

112 *Cryptococcus neoformans* var. *grubii* can be divided into three molecular types, or lineages:
113 VNI, VNII and VNB (Litvintseva et al., 2006; Meyer et al., 1999, 2009). The VNI and VNII
114 lineages are isolated globally, while the VNB lineage is predominantly located in sub-
115 Saharan Africa (Litvintseva et al., 2006), although there is some evidence for VNB occurring
116 in South America (Bovers et al., 2008; Ngamskulrungraj et al., 2009) and in the USA, Italy,
117 and China in AD hybrid isolates (Litvintseva et al., 2007). Apart from clinical isolation, the
118 VNI lineage is primarily associated with avian excreta (Lugarini et al., 2008; Nielsen et al.,
119 2007) while the VNB lineage is found mostly in association with specific tree species

120 predominantly mopane trees (Litvintseva and Mitchell, 2012; Litvintseva et al., 2011). These
121 and recent studies have shown that VNI infections are associated with urbanized
122 populations where an avian-associated reservoir, pigeon guano, is also found, while the
123 VNB lineage is widely recovered in the African arboreal environment (Litvintseva et al.,
124 2011; Vanhove et al., 2017).

125 Mating in *C. neoformans* occurs between cells of opposite mating types (*MATa* and *MAT α*)
126 (Kwon-Chung, 1975, 1976), although unisexual mating can also occur (Lin et al., 2005).
127 *MAT α* isolates are capable of unisexual mating both within and between the two serotypes
128 (Lin et al., 2005, 2007), and recombination was shown to occur at similar levels in bisexual
129 and unisexual mating in serotype D isolates (Desnos-Ollivier et al., 2015; Sun et al., 2014).
130 Due to the rarity of *MATa* isolates of both serotypes in the environment (Lengeler et al.,
131 2000a; Litvintseva et al., 2003; Viviani et al., 2001), unisexual mating may have evolved to
132 enable meiotic recombination and genetic exchange between isolates. Several studies have
133 found evidence of recombination within VNI, VNII, and VNB populations although not
134 between these lineages (Bui et al., 2008; Litvintseva et al., 2003, 2005).

135 An additional level of genome diversity detected in *C. neoformans* var. *grubii* includes the
136 presence of cryptic diploid isolates and variation in the copy number of individual
137 chromosomes or regions. Close to 8% of *C. neoformans* var. *grubii* global isolates appear
138 diploid; these isolates contain the *MAT α* locus and many appear autodiploid, thought to
139 result either from endoreduplication or self-mating (Lin et al., 2009). While the vast majority
140 of serotype A or D isolates appear haploid, individual chromosomes can be present at
141 diploid or triploid levels (Hu et al., 2011). For chromosome 1, a specific advantage of
142 aneuploidy is copy number amplification of the azole drug targets or efflux transporters,
143 associated with drug resistance (Sionov et al., 2010). While the specific selective advantage
144 of other chromosomal aneuploidies is unknown, same-sex mating of *MAT α* isolates
145 generates aneuploid progeny at high frequency, some of which also exhibit azole resistance
146 (Ni et al., 2013). Titan cells, polyploid yeast cells produced in the lung of infected animals,
147 also generate aneuploid progeny under stress conditions (Gerstein et al., 2015).

148 Previous studies examining the global population structure of *C. neoformans* var. *grubii* have
149 used typing methods for a few genetic loci or focused on particular geographical regions or
150 countries (Hiremath et al., 2008; Khayhan et al., 2013; Litvintseva et al., 2006; Oliveira et al.,
151 2004). Recent approaches have applied whole genome sequencing (WGS) to trace the
152 microevolution of *Cryptococcus*, identifying variation that occurs during the course of
153 infection (Chen et al., 2017; Ormerod et al., 2013; Rhodes et al., 2017) or in the environment
154 (Vanhove et al., 2017). Here, we use WGS of 188 isolates to provide a comprehensive view

155 of the population variation between the three major lineages; the sequenced isolates were
156 selected to represent the diversity of *C. neoformans* var. *grubii* including each of the three
157 major lineages and global geographical sampling. We identify contributions to genomic
158 diversity generated through inter-lineage meiotic exchange to create haploid hybrids,
159 generation of AD diploid hybrids, and regional copy number amplification. Furthermore, we
160 finely analyze the phylogenetic relationships and trace the evolution of *C. neoformans* var.
161 *grubii*, at the global population level.

162

163 **Methods**

164 Isolate selection

165 A total of 188 *C. neoformans* var. *grubii* isolates were selected from previous studies, which
166 include 146 clinical isolates, 36 environmental isolates, 4 animal isolates and 2 isolates of
167 unknown isolation source; these isolates were collected from 14 different countries:
168 Argentina, Australia, Botswana, Brazil, China, Cuba, France, India, Japan, South Africa,
169 Tanzania, Thailand, Uganda and USA (**Table S1**). Most of the clinical isolates were isolated
170 from the cerebrospinal fluid of patients. Eight of the 36 environmental isolates were isolated
171 from pigeon guano, and most of the remaining isolates were collected from Mopane and
172 other tree species.

173 Details of clinical trials and ethical review

174 French isolates were collected during the Crypto A/D study (Dromer et al., 2007). The study
175 was approved by the local ethical committee and reported to the French Ministry of Health
176 (registration # DGS970089). For clinical trials undertaken in South Africa (Bicanic et al.,
177 2007, 2008; Jarvis et al., 2012; Loyse et al., 2012) and Thailand (Brouwer et al., 2004),
178 ethical approval was obtained from the Wandsworth Research Ethics Committee covering St.
179 George's University of London. Local ethical approval was obtained from the University of
180 Cape Town Research Ethics Committee in South Africa and the ethical and scientific review
181 subcommittee of the Thai Ministry of Public Health. Clinical isolates from India were
182 collected during routine diagnostic service; local ethical approval was obtained from the
183 Institutional Ethical Committee of Vallabhbhai Patel Chest Institute, University of Delhi, India.

184 Fluconazole sensitivity testing

185 Fluconazole MICs were determined for two isolates by the NHLS laboratory in Green Point,
186 Cape Town using the E-test method (Biomérieux) (Bicanic et al., 2006).

187

188 DNA isolation and sequencing

189 Each yeast isolate was recovered from a freezer stock and purely cultured on an YPD or SD
190 agar plate for 48-60 h. Next, a single colony was inoculated to another YPD plate and
191 cultured for 24 h. Approximately 100 µl of yeast cells were used for DNA isolation using the
192 MasterPure yeast DNA purification kit (Epicenter, Madison, WI) according to the
193 manufacturer's instructions. Alternatively, a single colony was inoculated into 6ml YPD broth
194 supplemented with 0.5M NaCl and cultured for 40 hours at 37°C, prior to extraction using the
195 MasterPure Yeast DNA purification kit (Epicentre) as previously described (Rhodes et al.,
196 2017).

197 DNA was sequenced using Illumina technology; for each isolate, a small insert library was
198 constructed and used to generate between 14 and 150 million 101 bp paired-end reads per
199 isolate, which results in 56 to 603 fold average coverage of reads aligned to the H99
200 genome. In addition, large insert libraries were constructed for 15 isolates (**Table S4**) and
201 also used to generate 101 bp paired-end reads. Isolates were sequenced at Imperial
202 College London and the Broad Institute (**Table S1**).

203 Read alignment, variant detection, and ploidy analysis

204 Illumina reads were aligned to the *C. neoformans* var. *grubii* reference genome H99 (Janbon
205 et al., 2014) using the Burrows-Wheeler Aligner (BWA) 0.7.12 mem algorithm (Li, 2013) with
206 default parameters. BAM files were sorted and indexed using Samtools (Li et al., 2009)
207 version 1.2. Picard version 1.72 was used to identify duplicate reads and assign correct read
208 groups to BAM files. BAM files were locally realigned around INDELS using GATK (McKenna
209 et al., 2010) version 3.4-46 'RealignerTargetCreator' and 'IndelRealigner'.

210 SNPs and INDELS were called from all alignments using GATK version 3.4-46
211 'HaplotypeCaller' in GVCF mode with ploidy = 1, and genotypeGVCFs was used to predict
212 variants in each isolate. All VCFs were then combined and sites were filtered using
213 variantFiltration with QD < 2.0, FS > 60.0, and MQ < 40.0. Individual genotypes were then
214 filtered if the minimum genotype quality < 50, percent alternate allele < 0.8, or depth < 10.

215 In examining isolates with a high proportion of sites that were removed by these filters,
216 inspection of the allele balance supported that these isolates were diploid. For heterozygous
217 diploid isolates, haplotypeCaller was run in diploid mode. VariantFiltration was the same,
218 with the added filter of ReadPosRankSum < -8.0. Then for individual genotype filtration there
219 was no allele depth filter but otherwise was the same. The filters were kept as similar as

220 possible to maximize combinability. For AD hybrids, a combined reference of H99 (Janbon
221 et al., 2014) and JEC21 (Loftus et al., 2005) was used for alignment and SNP identification.

222 To examine variations in ploidy across the genome, the depth of bwa alignments at all
223 positions was computed using Samtools mpileup, and then the average depth computed for
224 5kb windows across the genome.

225 MAT locus determination

226 To evaluate the mating type alleles present in each isolate, Illumina reads were aligned
227 using bwa mem to a multifasta of both versions of the mating type locus (AF542529.2 and
228 AF542528.2 (Lengeler et al., 2000b)). Depth at all positions was computed using Samtools
229 mpileup, and then the average depth computed for the *SXI* and *STE20* genes for both
230 idiomorphs. Nearly all isolates showed unique mapping to either the *MATa* or *MAT α* alleles
231 of both genes; one isolate, Ftc158, showed significant mapping to both *MATa* and *MAT α* ,
232 though 2-fold more to *MAT α* . For the hybrid haploid isolates, the ancestry of the *MAT* locus
233 was determined from the Structure site by site output.

234 Genome assembly and annotation

235 Illumina sequence for each isolate was assembled using Allpaths (Maccallum et al., 2009)
236 for 36 isolates (see Table S4 for release numbers for each assembly) or SPAdes 3.6.0
237 (Bankevich et al., 2012) (with parameter `-careful`) for the remaining 3 isolates. Assemblies
238 with both fragment and jump libraries were more contiguous than those with fragment only
239 data (average of 84 or 561 scaffolds, respectively, **Table S4**). However there was little
240 difference in the total contig length between assemblies with or without jump data (average
241 18.4 Mb and 18.5 Mb, respectively, **Table S4**).

242 The predicted protein coding gene set for each assembly was generated by combining three
243 primary lines of evidence. Genes were transferred to each new assembly from the well
244 annotated H99 assembly (Janbon et al., 2014) based on whole genome nucleotide
245 alignments from nucmer. Genemark-ES (Ter-Hovhannisyan et al., 2008) was run on each
246 assembly to generate a de novo set of calls. These two sets were combined and improved
247 using PASA (Haas et al., 2008) with RNA-Seq data of three in vitro conditions (YPD, Limited
248 media, and Pigeon guano) generated for H99 (Janbon et al., 2014) and for the VNB isolate
249 Bt85 also input. Repetitive elements were removed from the gene set based on
250 TransposonPSI (<http://transposonpsi.sourceforge.net/>) alignments or PFAM domains found
251 only in transposable elements. The filtered set was assigned sequential locus identifiers

252 across each scaffold. The average number of 6,944 predicted genes across all assemblies
253 (**Table S4**) is close to the 6,962 predicted on the H99 reference.

254 Ortholog identification and comparison

255 To identify orthologs across the set of 45 *Cryptococcus* genomes (**Table S4**), proteins
256 clustered based on BLASTP pairwise matches with $\text{expect} < 1\text{e-}5$ using ORTHOMCL v1.4 (Li
257 et al., 2003). To identify orthologs specific to each of the serotype A lineages, we required
258 that genes were present in 90% of the assembled genomes for VNI (36 or more) or VNB (8
259 or more) or all VNII (3 genomes). To confirm that orthologs were missing in the other two
260 lineages, synteny was examined around each gene; in some cases this identified candidate
261 orthologs missed by OrthoMCL, which were confirmed by BLASTP similarity and removed.

262 Phylogenetic analysis

263 A phylogeny for the sets of 159 or 164 isolates was inferred from SNP data using RAxML
264 version 8.2.4 (Stamatakis, 2014) with model GTRCAT and 1,000 bootstrap replicates. A
265 separate analysis of the phylogenetic relationship based on gene content included 40 *C.*
266 *neoformans* var. *grubii* serotype A genomes (28 VNI, 3 VNII, and 9 VNB), 1 *C. neoformans*
267 var. *neoformans* serotype D genome (JEC21), and 4 *C. gattii* genomes (WM276, R265,
268 CA1873, and IND107) (**Table S4**). The total of 4616 single copy orthologs identified in all
269 genomes were aligned individually with MUSCLE (Edgar, 2004) at the protein level,
270 converted to the corresponding nucleotide sequence to maintain reading frame alignment,
271 poorly aligning regions removed trimal (Capella-Gutiérrez et al., 2009), and invariant sites
272 removed. A phylogeny was inferred using RAxML version 7.7.8 in rapid bootstrapping mode
273 with model GTRCAT and 1,000 bootstrap replicates.

274 Population structure

275 To examine major population subdivisions, we examined how isolates clustered in a
276 principal components analysis (PCA). SNP calls for all the isolates were compared using
277 SMARTPCA (Patterson et al., 2006). To identify the major ancestry subdivisions and their
278 contributions to the isolates appearing at intermediate positions in the PCA, a total of
279 338,562 randomly subsampled positions containing variants in at least two isolates and less
280 than 5% missing data were clustered using the Bayesian model-based program
281 STRUCTURE v2.3 (Pritchard et al., 2000) in the site-by-site mode. Ancestry was plotted
282 across the genome for each isolate using the matplotlib plotting package in Python.

283 For analysis of *C. neoformans* var. *grubii* diploid isolates (**Table S3**), diagnostic SNPs for
284 VNB and VNII were present exclusively in the respective group, and called for all VNB, VNII,

285 and ≥ 100 VNI isolates. Diagnostic SNPs for VNI were present exclusively in VNII and VNB,
286 and called for all VNB, VNII, and ≥ 100 VNI isolates.

287 Population genetic measures including P_i , F_{ST} , and Tajima's D were calculated using
288 popGenome (Pfeifer et al., 2014). d_N and d_S measures were calculated from fixed SNPs in
289 each lineage using codeml version 4.9c (Yang, 2007). To examine the distribution of the
290 alleles within VNB, we first identified 445,193 alleles private to VNB (present in at least 1
291 VNB isolate and no VNI or VNII isolates). We subdivided VNB into four clades (VNBI-South
292 America, VNBI-Africa, VNBII-South America, and VNBII-Africa) and calculated the number
293 of those private alleles unique to each clade (present in that one clade and no others) and
294 shared across VNB groups or geography (present in the two compared clades but no others).
295 The Mantel test was conducted using the center-point of each country to determine
296 distances between isolates and the number of SNPs between each pairwise set of isolates.
297 The test was conducted using available Python software
298 (<https://github.com/jwcarr/MantelTest>) with 1000 permutations and the upper tail test of
299 positive correlation.

300 Linkage disequilibrium

301 Linkage disequilibrium was calculated in 500 bp windows of all chromosomes except for the
302 ~ 100 kb mating type locus on chromosome 5 with vcfTools version 1.14 (Danecek et al.,
303 2011), using the `--hap-r2` option with a minimum minor allele frequency of 0.1.

304

305 Population inference by fineStructure

306 Model-based clustering by fineStructure (Lawson et al., 2012) assigns individuals to
307 populations based on a coancestry matrix created from SNP data, using either Markov chain
308 Monte Carlo or stochastic optimisation. The algorithm uses chromosome painting, which is
309 an efficient way of identifying important haplotype information from dense data, such as SNP
310 data, and efficiently describes shared ancestry within a recombining population. Each
311 individual is painted using all the other individuals as donors. For example, if an isolate x is
312 clonal and a donor, the clonally related recipients will receive almost all of their genetic
313 material from isolate x , and its closest relatives. This approach has been applied to analyze
314 recombination in fungal (Engelthaler et al., 2014) and bacterial studies (Yahara et al., 2013).

315

316 fineStructure analysis (Lawson et al. 2012) was performed using an all lineage SNP matrix,
317 with one representative of each clonal VNI population in order to infer recombination,
318 population structure, and ancestral relationships of all lineages. A separate analysis of all
319 VNI lineage isolates was also performed. This approach was based on the presence or
320 absence of shared genomic haplotypes. ChromoPainter reduced the SNP matrix to a

321 pairwise similarity matrix under the linked model, which utilises information on linkage
322 disequilibrium, thus reducing the within-population variance of the coancestry matrix relative
323 to the between-population variance. Since the MAT idiotypes introduce large bias into SNP
324 analysis, they were removed to enable characterisation of more defined populations. There
325 was no significant loss of sharing of genetic material when compared to retaining the MAT
326 locus.

327

328 **Results**

329 **Population subdivisions and detection of genetic hybrids**

330 To examine the evolution of *C. neoformans* var. *grubii*, we sampled the population by
331 sequencing the genomes of 188 isolates (**Table 1, Table S1**) representing each of the three
332 major genetic subpopulations (VNI, VNII, and VNB) previously defined using multi-locus
333 sequence typing (MLST) (Litvintseva et al., 2006; Meyer et al., 2009). These isolates are
334 geographically diverse, originating from North America, South America, the Caribbean, Asia,
335 Europe, and Africa (**Table S1**). The VNI global lineage is the most geographically diverse,
336 whereas VNII is represented by a smaller number of locations and VNB appears most highly
337 prevalent in southern Africa. For VNI and VNB, both clinical and environmental isolates were
338 included, with 25 VNI isolates originating from avian guano or trees and 8 VNB isolates from
339 trees or other environmental sources (**Table S1**). For each isolate we identified SNPs using
340 GATK by aligning Illumina reads to the H99 reference genome assembly (**Methods**, (Janbon
341 et al., 2014)). Whereas 164 isolates appeared haploid, 24 isolates were determined to be
342 heterozygous diploids (**Methods, Table 1**) and analyzed separately. An initial phylogeny of
343 the 164 haploid isolates separated the three lineages but intermediate placement of five
344 isolates suggested the presence of hybrid haploid genotypes (**Figure S1**). As the
345 phylogenetic placement of such hybrid isolates is complicated by recombination, we
346 removed these isolates from the phylogenetic analysis and analyzed them using alternative
347 approaches (see below).

348 A phylogeny inferred from the SNPs for all non-hybrid isolates strongly supports the
349 three major lineages of *C. neoformans* var. *grubii*: VNI, VNII, and VNB (**Figure 1**). Of these
350 159 isolates, only 6 (4%) contain the rare *MATa* allele, including four VNB isolates (Bt63,
351 Bt85, Bt206, and CCTP15) and two VNI isolates (125.91 and Bt130). Based on these whole
352 genome SNP comparisons, none of these *MATa* isolates appeared highly related to each
353 other or to any *MATa* isolate. The two VNI *MATa* isolates are well separated within this
354 group, with Bt130 found in a subgroup of African isolates and 125.91 most closely related to
355 a pair of isolates from Africa and North America (**Figure 1**). Phylogenetic analysis showed

356 that VNB has the highest diversity between isolates, showing the longest tip branches
357 compared to VNI or VNII. In addition, VNB consisted of two diverged subgroups, VNBI and
358 VNBI, as suggested previously by MLST (Chen et al., 2015; Litvintseva et al., 2006, 2011)
359 and genomic analysis (Desjardins et al., 2017; Vanhove et al., 2017).

360 To better understand the population structure of the three lineages and identify potential
361 inter-lineage recombination, we compared results of two independent approaches. First, we
362 used principle components analysis (PCA) to identify the major groups in the population
363 using the SNP data. By comparing the SNP variants across isolates using PCA, we found
364 there are three major clusters corresponding to the VNI, VNII, and VNB lineages (**Figure 2**).
365 The five isolates that showed intermediate positions in phylogenetic analysis (**Figure S1**)
366 also appeared at intermediate positions by PCA, placed between VNI and VNB. In addition,
367 two isolates were separated from the VNII cluster and shifted towards the VNB cluster. All of
368 these seven isolates were collected from southern Africa, and all had a clinical origin except
369 isolate Ftc260-1, which was isolated from the environment (**Table S1**). Of the seven, two
370 sets of isolates share nearly identical ancestry ratios and appear closely related on the
371 phylogenetic tree. Isolates Bt131, Bt162, and Bt163 differed by an average of only 39 SNP
372 positions; similarly CCTP51 and MW_RSA852 differed by 200 SNP positions, suggesting
373 these five isolates are descended from two hybridization events. Therefore, four unique
374 hybridization events were detected in total, three for VNI-VNB and one for VNII-VNB. While
375 the basal branching VNB isolates from Brazil could suggest a hybrid ancestry, all appear to
376 be uniformly VNB (>99% of sites).

377 Next, we identified the ancestry contribution of each isolate using STRUCTURE with three
378 population subdivisions. This confirmed that most isolates have a single dominant ancestry
379 assigned to the VNI, VNB, and VNII lineages. In addition, the isolates with intermediate
380 positions indicated by PCA were found to have mixed ancestry contributions by
381 STRUCTURE. SNP sites for the VNI-VNB hybrids contain an average of 40.8% VNI
382 ancestry and 59.2% VNB ancestry whereas the VNII-VNB hybrids have 85.8% VNII and
383 14.2% VNB ancestry (**Table S2**). The similar fraction of ancestry in the VNI-VNB hybrids
384 suggests they could be recent mixtures of the two lineages, whereas the VNII-VNB hybrids
385 may be more ancient mixtures with additional crosses to VNII isolates biasing the final ratio
386 of parental SNPs.

387 **Evidence of recent meiotic exchange generating haploid hybrids**

388 To examine the degree of intermixing of ancestry for these hybrid genotypes across the
389 genome, we identified the most likely ancestry for each SNP site using the site-by-site mode
390 in STRUCTURE. Selecting positions where the ancestry assignment was most confident

391 (0.9 or greater, **Methods**), we examined the distribution of these sites by ancestry across
392 the fourteen chromosomes (**Figure 3**). Each of the three VNI-VNB hybrids displayed
393 different patterns of large regions corresponding to a single ancestry. For example,
394 chromosome 1 has three large blocks of different ancestry in Bt125, four in Bt131, and two
395 in Ftc260-1 (**Figure 3A-C**). While all chromosomes contained regions of both VNI and VNB
396 ancestry groups in Bt125 and Ftc260-1, two chromosomes of Bt131, chromosome 6 and 9,
397 have only large regions of VNB ancestry. By contrast, CCTP51, which contains a lower
398 fraction of the second ancestry (VNB), appears more highly intermixed with smaller ancestry
399 blocks (**Figure 3D**). Notably, three of the four unique genotypes (Bt131, CCTP51, and
400 Ftc260-1) contain the rare *MATa* locus; in all *MATa* isolates, the mating type locus region is
401 of VNB ancestry, whereas the mating locus region in the *MAT α* isolate (Bt125) is of VNI
402 ancestry (**Methods**). Overall these patterns suggest a recent hybridization of VNI and VNB
403 isolates, with recombination during meiosis generating chromosome-wide intermixing
404 resulting in distinct parental haplotype blocks. In Bt125, a 205 kb region of scaffold 6 is
405 present at nearly twice (1.92 fold) the average depth. Otherwise this isolate and the other six
406 hybrid isolates were found to contain even levels of ploidy across the 14 chromosomes
407 based on read depth.

408 For the three VNI-VNB hybrids showing large ancestry blocks, we also utilized the site
409 ancestry predictions to finely map the genotypes within each population. Given the roughly
410 equal contribution of the two ancestry sites and the large block size for each in these
411 genomes, we hypothesized that these hybrids could have resulted from recent mating of one
412 genotype of each lineage, which we could reconstruct using separate phylogenies of each
413 site class. For each genotype, sites mapped to either the VNI or VNB ancestry were
414 selected and a separate phylogeny constructed for each of these two sets of sites. For VNI
415 ancestry sites, these isolates had very different genotypes, with Ftc260-1 most closely
416 related to a diverse set of African isolates in VNI, whereas both Bt125 and Bt131 are more
417 closely related to highly clonal clades of VNI isolates (**Figure S2A,C,E**). Similarly for a
418 separate phylogenetic analysis of VNB ancestry sites, Bt125 and Bt131 were placed within
419 the VNBII subclade of VNB while Ftc260-1 was placed in VNBI (**Figure S2B,D,F**). This
420 supports that these three hybrids originated from very different genotypes of VNI and VNB
421 parental isolates.

422 **Diploid isolates and genome plasticity**

423 As noted above, a total of 24 sequenced isolates displayed heterozygous SNP positions
424 across the genome. Four of these isolates had higher rates of polymorphism overall and
425 appear to be hybrids within or between VN lineages (Bt66, Cng9, PMHc.1045.ENR.STOR,

426 and 102-14) (**Figure S3**). Each of these isolates contain two copies of the *MAT α* mating type
427 locus which show similar levels of heterozygosity as the rest of the genome, suggesting that
428 these diploids arose from same sex mating of two *MAT α* parental isolates with different
429 genotypes. In addition, 11 serotype A diploids showed very low rates of heterozygosity
430 (**Figure S3**), consistent with AFLP and MLST-based evidence that they arose from
431 endoreduplication or self-mating (Lin et al., 2009). The remaining isolates include eight
432 serotypeA/serotypeD diploids, of which seven contain both *MAT α* and *MAT α* mating types
433 and one is homozygous for the *MAT α* locus, and one serotype A/*Cryptococcus gattii* hybrid
434 containing two copies of *MAT α* .

435 All types of diploid isolates in our set, including A/A diploids, exhibit regions of loss of
436 heterozygosity (LOH) in the genome, where alleles of only one parental isolate are present.
437 Three of the A/A diploids (Bt66, Cng9, and 102-14) are heterozygous throughout nearly all of
438 the genome; Cng9 exhibited only a small LOH region at the start of chromosome 2, which
439 also has haploid levels of genome coverage. Isolate PMHc1045 by contrast has large LOH
440 regions on six scaffolds, including a 1.1 Mb region of chromosome 6 (**Figure S3**). Some of
441 these regions of LOH in PMHc1045 are linked to aneuploid chromosome segments,
442 including a region of chromosome 12 reduced to haploid levels and or triploid levels of the
443 region adjacent to a LOH on chromosome 6. All LOH regions are telomere-linked,
444 reminiscent of what has previously been reported across diverse isolates of *Candida*
445 *albicans* (Hirakawa et al., 2015).

446 We next inferred the ancestry of the two parental isolates contributing to the A/A hybrids by
447 examining the frequency of SNP alleles that are highly predictive for VNI, VNII, or VNB
448 (**Methods**). Three of the isolates (Cng9, PMHc1045, and 102-14) have similar frequencies
449 of such VNII and VNB alleles, whereas Bt66 is comprised of VNI and VNB predictive alleles
450 (**Table S3**). Comparing Cng9 and PMHc1045 directly, 89.2% of variant sites are identical;
451 this fraction increases to 97.3% when LOH regions are excluded and a similar fraction of
452 sites are shared with 102-14. Notably, LOH has resulted in a mixing of genotypes;
453 examining predictive alleles for each of the seven LOH regions of PMHc1045 (**Figure S3**)
454 revealed two regions encompassing 1.4% of the genome share the highest fraction of
455 private alleles with other VNB isolates whereas the remaining five regions encompassing
456 10.2% of the genome share most private alleles with other VNII isolates. By contrast, Cng9
457 has only a single small region of LOH that does not overlap with any of the seven LOH
458 regions in PMHc1045. Thus, LOH has led to large differences between otherwise highly
459 similar Cng9 and PMHc1045 isolates and resulted in blended ancestry by converting regions
460 to each of the two parents in PMHc1045.

461 The eight AD hybrids also showed evidence of even more extreme aneuploidy and LOH
462 related to loss of one of the two parental chromosomes. All isolates displayed evidence of
463 aneuploidy, by examining read coverage across both the H99 serotype A and JEC21
464 serotype D reference genomes (**Figure S4**). While some isolates have retained
465 chromosomes of both A and D origin, others have lost a chromosome from one parent and
466 duplicated the corresponding chromosome of the other (**Figure 4, Figure S4**). For example
467 in RCT14, two copies of chromosome 1 are present but both have serotype A origin;
468 similarly in IFNR21, both copies of chromosome 10 have serotype D origin. Both of these
469 isolates display additional aneuploidies, with 3 copies of some chromosomes. Notably,
470 CCTP50 appears mostly triploid, with either 2:1 or 1:2 ratios of the A:D ratio for each
471 chromosome (**Figure 4**); this pattern is also observed in IFN26 (**Figure S4**). In IFN-R26, loss
472 of chromosome 4 in JEC21, balanced by gain of chromosome 5 in H99 (**Figure S4**), has
473 resulted in a *MATa/MATa* genotype. While the mating type of the original JEC21 parent can
474 not be determined, this suggests that generation of *MATa/MATa* diploids can occur via
475 chromosome loss and duplication. All other isolates are *MATa/MAT α* , suggesting that they
476 originated from opposite sex mating. While diploid AD hybrids have been isolated from both
477 environmental or clinical sources (Litvintseva et al., 2006), all eight AD hybrids in our set are
478 of clinical origin.

479 To examine the diversity of these AD hybrids, SNPs were identified by comparison to a
480 combined A (H99) and D (JEC21) genome reference. Phylogenetic analysis of A and D
481 genome SNPs revealed that both the A and D copies of each hybrid are closely related for
482 these isolates (**Figure S5**). On average, the A genomes differ by 6,108 SNP positions and
483 the D genomes by 3,935 SNP positions. The A genomes are from the VNB lineage, most
484 closely related to Bt206 in our analysis (**Figure S5**). The low diversity of both the A and D
485 genomes between isolates suggests that this set of 8 AD hybrids may have originated from
486 a single hybrid isolate or from a set of closely related A and D parental isolates.

487 **Chromosomal copy number variation**

488 On a smaller scale than whole-genome hybridization, chromosomal copy number variants
489 appear to be common in *C. neoformans* and may be an adaptive mechanism for virulence
490 (Rhodes et al., 2017). In the set of 164 primarily haploid isolates, 25 exhibited whole or
491 partial chromosomal aneuploidies (**Figure S6**). In 13 of the 25 isolates, an entire
492 chromosome or region thereof showed a doubling of sequencing coverage, consistent with a
493 diploid chromosome in an otherwise haploid isolate. The remaining 12 isolates show a 50%
494 gain in coverage better explained by a diploid isolate with a triploid chromosome or region.

495 These likely diploid isolates do not display heterozygous base calls, suggesting a recent
496 endoreduplication of the genome and associated aneuploidy of additional chromosomes.

497 Aneuploidies of particular chromosomes may provide a specific biological advantage or
498 alternatively be better tolerated. In general, the smallest chromosomes (12 and 13) are the
499 most frequently observed to exhibit aneuploidy (**Figure S6**). Several isolates have an
500 increased copy number of chromosome 1; amplification of the lanosterol-14- α -demethylase
501 *ERG11* and the major efflux transporter *AFR1* located on chromosome 1 can confer
502 resistance to azole drugs (Sionov et al., 2010). Of the four isolates that contain chromosome
503 1 aneuploidies, either *ERG11* (CCTP34) or *AFR1* (IFN-R11 and RCT6) or both genes
504 (CCTP9) are present at elevated copy number. The elevated copy number of *AFR1* appears
505 correlated with increased drug resistance; both CCTP9 and RCT6 displayed fluconazole
506 MIC values of 256 ug/ml, whereas CCTP34 appeared more susceptible at an MIC of 8 ug/ml
507 (**Methods**). Notably, all of the isolates with chromosome 1 aneuploidies are of clinical origin,
508 as are 24 of all 25 isolates with detected aneuploidies (**Figure S6, Table S1**). Of the seven
509 isolates with hybrid ancestry, only Bt125 included a small region of chromosome 6 at higher
510 copy number; otherwise, this and the other hybrid isolates appeared to be haploid. Across
511 the diploid and haploid isolates, we detected aneuploidies affecting all chromosomes
512 (**Figures S3, S4, and S6**).

513

514 **Conservation of gene content and structure across lineages**

515 To examine the extent of gene content variation across the three major lineages of *C.*
516 *neoformans* var. *grubii*, we assembled and annotated genomes of 39 representative isolates
517 (**Methods**). Previously a high quality reference genome was produced for the H99 VNI
518 isolate (Janbon et al., 2014); our data set includes new annotated assemblies for 9 diverse
519 VNB isolates, 27 VNI isolates, and three VNII isolates (**Table S4**). The gene sets across all
520 40 assemblies (including H99) were compared to each other and to those of four *C. gattii*
521 (representing VGI, VGII, VGIII, and VGIV) and one *C. neoformans* var. *neoformans*
522 (serotype D) reference genomes (**Methods**) in order to evaluate gene conservation. Based
523 on orthologs identified across these genomes (**Methods**), an average of 4,970 genes are
524 conserved across all 45 compared *Cryptococcus* gene sets; within serotype A, an average
525 of 5,950 genes are conserved in all 40 genomes (**Figure S7**). A phylogeny inferred from
526 4,616 single copy genes supports VNII in an ancestral position relative to the more recently
527 diverging VNI and VNB (**Figure S7**; 100% bootstrap support), solidifying results previously
528 seen with targeted sequencing of 11 nuclear loci (Hagen et al., 2015).

529 Gene content is highly conserved across *C. neoformans* var. *grubii* with few examples of
530 genes specific to the separate lineages (**File S1**). Based on ortholog profiling, a total of 11
531 genes are specific to VNI, three specific to VNB, and 25 specific to VNII (**Table S5**). These
532 include two clusters of genes specific to VNI or VNII located within otherwise syntenic
533 regions of the genome (**Figure 5**). The cluster of five genes unique to VNI genomes include
534 a predicted haloacid dehydrogenase, an amidohydrolase and an allantoin permease, which
535 could be involved in uptake of uric acid products. The cluster of six genes unique to the VNII
536 genomes includes a predicted transcription factor, amino acid transporter, hydrolase,
537 dihydropyrimidinase, and oxygenase superfamily protein. While both clusters are also
538 missing from the JEC21 *C. neoformans* var. *neoformans* genome, the more distantly related
539 *C. gattii* genomes contain syntenic orthologs of all of the VNII-specific cluster genes and
540 between 1 and 3 non-syntenic orthologs of the VNI-specific cluster. These patterns suggest
541 gene loss and perhaps lateral transfer in some species and lineages account for these
542 differences. There was little other evidence of lineage-specific gene loss; orthologs missing
543 in only one lineage included only hypothetical proteins. In addition, we further searched for
544 genes with loss-of-function mutations in all members of each lineage using SNP data, to find
545 genes that may be disrupted but still predicted in the assemblies. However, we found no
546 convincing evidence of disrupted genes with known functions in all members of any of the
547 three lineages (**File S1**).

548 Given the high level of gene conservation between lineages, we sought to identify rapidly
549 evolving genes that might be involved in phenotypic differences between *C. neoformans*
550 lineages. For each gene, we built a consensus sequence for each lineage and then
551 calculated pairwise d_N and d_S of these fixed sites. As d_S was uniformly low throughout the
552 dataset due to limited genetic diversity, we identified differences in d_N , which measures both
553 the mutation rate and selection. The top 10 annotated genes with the largest d_N for each
554 pairwise comparison are shown in Table 2, and the three comparisons in total include 18
555 unique genes. The set is dominated by transcription factors (*GLN3*, *PDR802*, *SX11 α* ,
556 *YOX101*, and *ZNF2*) and transferases (*ATG2602*, *CDC43*, *GPI18*, *HOC1* and *RAM1*), many
557 of which have already been implicated in virulence (Esher et al., 2016; Jung et al., 2015; Lee
558 et al., 2015; Selvig et al., 2013; Wang et al., 2012) or resistance to oxidative stress (Jung et
559 al., 2015). In particular, *CDC43* and *RAM1* are both rapidly evolving; these genes represent
560 the two major independent methods of prenylation, key in proper subcellular localization of
561 many proteins, often to the membrane (Esher et al., 2016; Selvig et al., 2013). Other rapidly
562 evolving genes include β -glucan synthase *KRE63*, superoxide dismutase *SOD1*, and mating
563 regulator *SX11 α* , the latter of which is highly divergent between VNII and both VNI and VNB,
564 and could play a role in reproductive isolation of the VNII lineage.

565 **Population measures and biogeography**

566 Strikingly, recently identified VNB genotypes from South America are placed in the
567 phylogeny as basally branching clades for each VNB subgroup, which otherwise consist of
568 genotypes from Africa (**Figure 1**). All of the six South American VNB isolates contain the
569 *MAT α* genotype. By contrast, both VNI and VNII consist of more closely related though more
570 geographically diverse sets of isolates; one large clonal group is found in VNII, whereas
571 several are observed for VNI, which is oversampled owing to its higher prevalence in
572 patients and environments worldwide. Overall, VNB showed the highest average pairwise
573 diversity ($\pi=0.00736$), nearly four times the level in VNI ($\pi=0.00200$), with the lowest value
574 for VNII ($\pi=0.00105$) (**Table 3**). Genetic diversity within the VNB lineage was similar
575 between the South America and African isolates ($\pi=0.00727$ and 0.00736 , respectively).
576 However, genetic diversity of VNI isolates in India was lower than VNI isolates in Africa
577 ($\pi=0.00146$ and 0.00337). VNB also contained the largest fraction of private alleles
578 compared to VNI and VNII, reflecting the higher variation within VNB (**Table 4**). By contrast,
579 VNI and VNII had the highest number of fixed differences, reflecting the long branches
580 leading to these clades. The average divergence (d_{XY}) between lineages ranges is 0.012
581 comparing isolates from VNI and VNB and 0.015 for comparison of either to VNII (**Table 4**),
582 highlighting the low nucleotide divergence between the lineages. VNI and VNII were the
583 most differentiated of the three lineages as shown by pairwise whole genome fixation
584 indexes (F_{ST}) (Weir and Cockerham 1984). The highest average chromosome F_{ST} value is
585 0.874 between VNI and VNII isolates, while the average chromosome F_{ST} values of VNI-
586 VNB and VNB-VNII are 0.595 and 0.707 , respectively (**Table 4**).

587

588 To further examine the evolutionary history of the novel South American VNB isolates, we
589 subdivided VNB into four subclades (VNBI-South America, VNBI-Africa, VNBII-South
590 America, and VNBII-Africa) and calculated alleles unique to each subclade and shared
591 across VNB groups or geography (Methods). These subclades represent all combinations of
592 the two previously identified VNB groups (VNBI and VNBII) and the two geographies (South
593 America and Africa). One South American VNB isolate (V53), nested deeply within African
594 isolates on the phylogeny, was excluded from the analysis. Each of the four subclades
595 contained more unique alleles than were shared across either VNB group or geography
596 (**Figure 7**), suggesting both a high level of genetic diversity within each subclade and some
597 degree of reproductive isolation between them. Furthermore, there was greater number of
598 unique alleles shared within the VNB groups from different geographic regions than were
599 shared across VNB groups within the same geographic region (**Figure 7**). This
600 geographically and phylogenetically segregated diversity suggests that multiple ancient

601 migration events occurred between South America and Africa during the diversification of
602 VNB, followed by geographic isolation. In contrast, the VNI and VNII lineages showed a
603 pattern consistent with more rapid current migration, where isolates from different
604 geographic regions in many cases differed by fewer than 200 SNPs.

605 We next evaluated whether VNI and VNB showed a signal of genetic isolation by distance
606 using the Mantel test. In both VNI and VNB, genetic distance was significantly positively
607 correlated with geographic distance ($p = 0.0001$ and $p = 0.042$, respectively). When VNB
608 was separated into VNBI and VNBII, each lineage showed an even stronger signal ($p =$
609 0.0051 and $p = 0.0009$, respectively), suggesting much of the correlation seen within VNB is
610 representative of isolation within each subclade. Therefore, despite VNB showing signals of
611 more ancient migration while VNI shows signals of recent migration, both demonstrate
612 genetic substructure according to geography.

613 **Recombination between and within lineages**

614 The basal branching of Brazilian VNB isolates revealed in the phylogenetic analysis
615 suggested that South America could be a global center of *C. neoformans* var. *grubii* diversity.
616 To further investigate this hypothesis, and to explore recombination in the context of
617 population structure, we implemented the chromosome painting approach of fineStructure
618 (Lawson et al., 2012), which identifies shared genomic regions between individuals and
619 thereby ancestral relationships among individuals and populations. Our linked co-ancestry
620 model found the highest level of sharing among VNB isolates; in addition, there is evidence
621 of strong haplotype donation from South American VNB isolates (V2, V31, and V87) to all
622 other lineages and continents, suggestive of ancestral recombination (**Figure 6**).

623 Independent confirmation of ancestry using STRUCTURE confirmed that V87 includes
624 primarily VNB ancestry with ~1% VNI alleles (**Table S7**). Interrogating the chunk counts,
625 which are lengths of DNA shared by a donor to other individuals, and lengths produced by
626 fineStructure revealed that the haplotype chunks donated by these 'ancestral' isolates were
627 substantially higher than seen for other isolates, with other African VNB isolates receiving
628 significant chunks and lengths (Bt102, Bt63, Bt85, Tu229-1, Tu360-1, Tu369-1, and Tu401-
629 1) from the South American VNB isolates. Isolate V53 donated less strongly than these
630 three isolates to all lineages. Other South American VNB isolates (WM 1408 and V17)
631 donated strongly to specific lineages: WM 1408 to VNII and VNB, whilst V17 donated to VNI
632 and VNB. However, these findings for WM 1408 and V17 were not corroborated using
633 STRUCTURE. Despite their allocation to separate VNB subpopulations, V2 and V17 (VNB-I
634 and VNB-II respectively) donate the most genetic material (when interrogating the chunk
635 counts) to VNI isolates in Africa, India, and Thailand.

636

637 Within the VNI lineage, fineStructure analysis identified a subset of isolates with a high
638 frequency of haplotype sharing (**Figure 8**). Notably, a group of African (Tu259-1, 125.91,
639 RCT52, Bt100, Bt207 and Bt30) and Indian (INCr213 and INE071) isolates show strong
640 haplotype donation with many other VNI isolates, suggestive of ancestral recombination
641 events. These isolates are dispersed over four subpopulations within the VNI lineage.
642 Though the geographical distance between these populations should preclude frequent
643 intermixing, these isolates from Africa and India may include a higher fraction of ancestral
644 alleles, leading to a lack of phylogeographic structure among these highly geographically
645 distinct populations.

646

647 Finding that ancestral recombination in the VNB lineage contributed to VNI lineage diversity
648 suggested that there could be a signature of admixture linkage disequilibrium (LD) in these
649 two populations. Linkage disequilibrium differs between lineages (**Figure S8**), with VNII LD
650 decaying slowly with physical distance, and manifesting an LD50 (where linkage
651 disequilibrium has decayed to half its maximum value) at >150 kb. However, this value may
652 reflect the highly clonal nature and relatively small number of sequenced VNII isolates. LD
653 decay is relatively slow for VNI with an LD50 of 4,500 bp, whereas LD decays more rapidly
654 in the VNB lineage, with an LD50 of 1,500 bp. When separated into geographical origin of
655 isolation (**Figure S8** (b)), LD50 for South American VNB appears greater (> 150 kbp) than
656 that seen in African VNB (2,000 bp). The slower decay of LD in VNI and VNII relative to VNB
657 may reflect a lower frequency of sexual reproduction owing to the rarity of the *MATa*
658 idiomorph and therefore meiotic recombination would have fewer opportunities to break
659 apart LD blocks.

660

661 **Discussion**

662 This population genomic analysis of *C. neoformans* var. *grubii* has revealed new
663 biogeographic relationships and highlighted a complex history of hybridization events
664 between groups. Analysis of genome-wide variation of 188 geographically diverse isolates
665 greatly increases the resolution of the VNI, VNII, and VNB phylogenetic groups and
666 precisely measures the level of genetic differentiation between isolates within each group
667 and across geographic scales. This data supports a much higher diversity of isolates in the
668 VNB group compared to VNI and VNII isolates. Notably, we show that hybridization between
669 these groups can result in genome mixing suggestive of recent and ongoing meiotic
670 exchange, and introgression of smaller regions between lineages have been identified and
671 appear to perpetuate vertically (Desjardins et al., 2017). Therefore, although there is good

672 support for the separation of the groups based on phylogenetic analysis, the measures of
673 intermixing that we observe do not meet the strict requirements for species definition under a
674 Genealogical Concordance Phylogenetic Species Recognition (GCPSR) framework
675 (Dettman et al., 2003; Taylor et al., 2000). GCPSR defines phylogenetic species by
676 identifying the transition from genealogical concordance to conflict (reticulate genealogies)
677 as a means of determining the limits of species, a requirement that *C. neoformans* var. *grubii*
678 does not appear to satisfy owing to ongoing gene flow among the lineages. Similarly, a
679 recent taxonomic proposal to divide the *C. neoformans* and *C. gattii* species complexes into
680 seven monophyletic species did not subdivide *C. neoformans* var. *grubii* into separate
681 species; while VNI, VNII, and VNB were strongly supported clades in a multilocus phylogeny,
682 coalescent based approaches did not clearly support these three lineages as separate
683 species (Hagen et al., 2015). In addition, the inter-lineage recombination or hybridization
684 events may be a biological feature that extends across other lineages within the *C.*
685 *neoformans* and *C. gattii* species complexes (Farrer et al., 2015; Hagen et al., 2015),
686 prompting a need for wider investigation of the population genomic structure of the entire
687 complex using a rigorously-applied GCPSR framework to support formal changes in
688 taxonomy (Kwon-Chung et al., 2017).

689

690 The placement of isolates from Brazil at basal branching positions of the two VNB subclades
691 phylogenetically separates the South American and African isolates within both the VNBI
692 and VNBI groups. This finding, along with the presence of a large number of unique alleles
693 in each of these four subclades and strong haplotype sharing seen with fineStructure
694 analysis (**Figure 7**), suggests that there were ancient migrations of the VNB group between
695 Africa and South America following the initial divergence of VNBI and VNBI, but prior to
696 each group's radiation. This finding appears consistent with a prior report of diverse isolates
697 from Brazil in a new VNI genotype 1B (Oliveira et al., 2004). While the lack of a trustworthy
698 molecular clock combined with substantial rates of recombination currently precludes
699 confidently dating the time of divergence between VNB from South America and Africa, this
700 division clearly occurred after these continents split over 110 million years ago, and also
701 after VNB itself subdivided into two lineages – VNBI and VNBI. As is the case with VNI,
702 cross-Atlantic migration events may also have vectored VNB between these two continents.
703 Despite evidence for these migration events, the majority of VNI and VNBI migrations were
704 likely much more recent than is seen with VNB, with nearly clonal isolates of VNI and VNBI
705 found in disparate geographic regions. The presence of one South American VNB isolate
706 (V53) that nests within African isolates on the phylogeny suggests a limited number of more
707 recent migration events may be occurring between the two regions even within VNB, despite
708 the large degree of reproductive isolation that we observed. Identification of additional South

709 American VNB isolates is necessary to determine their diversity and relationship to isolates
710 from African continental regions. Although the sequenced isolates all contain the *MAT α*
711 genotype, our sample size was small and likely under-represents the true diversity of this
712 lineage in South America and the ecological reservoirs that it occupies.

713 Given the propensity of *C. neoformans* var. *grubii* VNI and VNII for having an environmental
714 reservoir in bird excreta (unlike VNB which is principally associated with arboreal reservoirs
715 (Litvintseva et al., 2011; Vanhove et al., 2017), it has been proposed that radiations of birds,
716 likely pigeons, globally dispersed *C. neoformans* var. *grubii* from a genetically diverse
717 population in southern Africa (Litvintseva et al., 2011) resulting in an expansion of the *C.*
718 *neoformans* var. *grubii* VNI out of Africa. Litvintseva et al. (2011) hypothesized that this “out-
719 of-Africa” model for the evolution of VNI explains the origin of the global VNI population.
720 Other studies showing lower genetic diversity of VNI populations in Southeast Asia
721 (Simwami et al., 2011) and in South America (Ferreira-Paim et al., 2017) further support an
722 African origin of *C. neoformans* var. *grubii*. An alternative explanation for the higher diversity
723 of African VNI could be that this lineage originated elsewhere and became more diverse in
724 this continent by mating with the ‘native’ VNB population or due to other factors. Our
725 analysis did not find a large subset of VNB alleles within the African VNI isolates based on
726 ancestry analysis. In addition, we found one VNI subclade composed mostly of African
727 isolates that appears to be recombining at higher frequency than other VNI groups. The
728 phylogenetic intermixing of isolates from India and Africa strongly support the hypothesis
729 that there is long-range dispersal and ancient recombination in environmental populations in
730 India and Africa, indicative of multiple migratory events across time and into the present. Did
731 VNI therefore evolve ‘out-of-Africa’? Further sampling of environmental isolates from across
732 South America and more diverse regions of Africa, as well as correct estimation of the
733 mutation rate in *C. neoformans* var. *grubii* to allow calibration of a molecular clock, is needed
734 to further test this hypothesis.

735 While gene content is very similar across the *C. neoformans* var. *grubii* lineages, we found
736 examples of lineage specific genes including clusters unique to VNI or VNII. While this
737 suggests that the *C. neoformans* var. *grubii* gene inventory based on H99 (Janbon et al.,
738 2014) is largely representative of all lineages, additional genes specific to VNII and VNB are
739 important to consider in studies focusing on isolates of these lineages. Differences in gene
740 expression may also differentiate the lineages, and it is important to note that these will
741 include lineage-specific genes that may contribute to variation in clinical profiles and
742 virulence that occur among lineages of *C. neoformans* var. *grubii* (Beale et al., 2015). In
743 addition, we found the most rapidly evolving genes between each of the lineages include
744 transcription factors and transferases, suggesting phenotypic diversity may be generated

745 through transcriptional reprogramming and protein modification rather than changes in gene
746 content. The *SX11* gene detected in comparisons of VNII with both VNI and VNB appears to
747 be highly substituted in the VNII lineage; this sequence divergence of *SX11* in VNII could
748 contribute to differences in mating with this group. Truncated alleles of *SX11* are frequently
749 observed in the serotype D *MAT α* chromosome of AD hybrids and suggested to contribute to
750 increased mating efficiency (Lin et al., 2007).

751 Our analysis revealed that hybrid isolates originate from multiple lineages, and resolved the
752 parental genotypes. Prior analysis with MLST loci suggested that some isolates contain a
753 mix of multiple genotypes (Chen et al., 2015; Litvintseva et al., 2003). However the
754 sensitivity and precision of these methods has been limited by the small number of loci
755 examined, the use of genes involved in virulence that may be under different selective
756 pressure, as well as incomplete lineage sorting in some groups. Analysis of genome-wide
757 variation revealed that some isolates appear to be a recent mix of different ancestries, based
758 on the detection of large blocks of sites with each ancestry; this could result from a small
759 number of crossing over events for each chromosome during meiosis. Other isolates contain
760 more highly intermixed ancestry across the genome and predominantly of a single ancestry;
761 these may have occurred by more historical hybridization followed by subsequent mating
762 within a single lineage group. The demonstration of genome mixing in hybrid isolates raises
763 interesting questions about whether such fundamentally new assortments of the three
764 lineages could generate genotypes with new phenotypes, which perhaps have a fitness or
765 selective advantage.

766 Analysis of hybrids between serotypes A and D revealed a remarkable degree of genome
767 reassortment. All of the 8 sequenced AD isolates show evidence of aneuploidy, affecting the
768 copy number of 12 of 14 serotype A derived chromosomes and all 14 serotype D derived
769 chromosomes. This is consistent with the high rate of AD isolate aneuploidy previously
770 reported using flow analysis of DNA content (Lengeler et al., 2001) or comparative genome
771 hybridization (Hu et al., 2008). For some chromosomes, only one parental genotype was
772 detected in a subset of five isolates; this includes a loss of the serotype D copy of
773 chromosome 1, as previously observed in analysis of three AD hybrid isolates (Hu et al.,
774 2008). However, we further find that loss of heterozygosity (LOH) in some cases is due to
775 partial copies of several chromosomes, suggesting that genomic instability in AD hybrids
776 may result in chromosomal breakage. LOH was also observed for smaller regions in diploid
777 AA hybrids. Similar LOH events are frequently observed in diploid fungi including *Candida*
778 *albicans* (Hirakawa et al., 2015) and may contribute to the generation of genetic diversity in
779 both species.

780 Aneuploidy was also commonly observed in the haploid *C. neoformans* var. *grubii* isolates.
781 Additional copies of regions of chromosome 1 that include *AFR1* or *ERG11* are associated
782 with drug resistance, though aneuploidies of additional chromosomes are also observed
783 (Sionov et al., 2010). Although functional significance of aneuploidy of other chromosomes is
784 less well understood, most of the isolates exhibiting aneuploidy are of clinical origin,
785 suggesting increased copy of other genes may provide an advantage or that there is higher
786 genome instability during infection. An isochromosome of the left arm of chromosome 12
787 that arose during infection has been reported (Ormerod et al., 2013) and chromosome 12
788 aneuploidy is widely seen in African patients with relapsed infections (Chen et al., 2017;
789 Rhodes et al., 2017) although the specific role of this duplication is unclear. Our data
790 suggests that there could be additional isochromosomes based on the detection of partial
791 chromosomes using sequencing read depth; alternatively these regions could be
792 represented in the genome as fusions with other chromosomes.

793 Previous studies of *C. gattii* have pointed towards South America as a source of the diversity
794 for the *C. gattii* VGII lineage (Engelthaler et al., 2014; Hagen et al., 2013). Given the shared
795 evolutionary history of *C. gattii* and *C. neoformans* var. *grubii* (Xu et al., 2000), South
796 America could also represent a major diversity center of *C. neoformans* var. *grubii*. Our data
797 suggests that *C. neoformans* var. *grubii* VNB isolates in both subgroups from South America
798 have undergone ancestral recombination events, donating genetic material to all lineages
799 across multiple geographical locations. Our study also provides clear evidence that
800 recombination is more limited by lineage than by geographic barriers; the transcontinental
801 nature of *C. neoformans* var. *grubii*, particularly the VNI and VNII lineages, supports the
802 hypothesis of historical or ongoing migration events to facilitate such recombination. Our
803 study identified recombination within the VNI and VNII lineages, where nearly all the isolates
804 contain the *MAT α* mating type. This suggests that mating likely occurs between *MAT α*
805 isolates, as is found in *C. neoformans* var. *neoformans* (Sun et al., 2014). Previous studies
806 have hypothesized that *C. neoformans* var. *grubii* can complete its sexual reproductive life
807 cycle in environmental niches, such as plants (Xue et al., 2007) and pigeon guano (Nielsen
808 et al., 2007; Vanhove et al., 2017). Our observations that all lineages of *C. neoformans* var.
809 *grubii* show the ability to widely disperse, recombine, and hybridize, across large geographic
810 distances, illustrates that this pathogen has a high degree of evolutionary plasticity.
811 Therefore, lineages that have not drifted in the frequency of their mating types are likely to
812 display higher rates of recombination and hybridization. These factors are likely related to
813 the success of *C. neoformans* var. *grubii* in infecting the immunosuppressed 'human
814 environment', thereby causing a high burden of mortality worldwide (Armstrong-James et al.,
815 2014).

816

817 **Acknowledgments**

818 We thank the Broad Institute Genomics Platform for generating DNA sequence for this study
819 and Jose Muñoz for helpful comments on the manuscript.

820 **Funding Statement**

821 This project has been funded in whole or in part with Federal funds from the National
822 Institute of Allergy and Infectious Diseases, National Institutes of Health, Department of
823 Health and Human Services, under grant number U19AI110818 and by the National Human
824 Genome Research Institute grant number U54HG003067 to the Broad Institute. Support to
825 J.R.P. came from Public Health Service Grants AI73896, AI93257. JR and MAB were
826 supported by a UK Medical Research Council Grant awarded to MCF, TB and TH (MRC
827 MR/K000373/1). MV was supported by a UK Natural Environment Research Council PhD
828 studentship. JH was supported by NIH grants AI39115-19 and AI50113-13. DL was funded
829 by Wellcome Trust Grant Number WT104125MA. The funders had no role in study design,
830 data collection and analysis, decision to publish, or preparation of the manuscript.

831 **Data access**

832 All sequence data from this study have been submitted to GenBank under BioProject ID
833 PRJNA 384983 (<http://www.ncbi.nlm.nih.gov/bioproject>); individual accession numbers are
834 listed in Supplemental Tables S1 and S4.

835 **Author contributions**

836 **Investigation:** JR, CAD, SMS, SS, CAC

837 **Validation:** JR, CAD, SMS, CAC

838 **Visualization:** JR, CAD, SMS, SS, CAC

839 **Writing – Original Draft Preparation:** JR, CAD, CAC

840 **Writing – Review & Editing:** JR, CAD, MCF, CAC, AA, MAB, DME, WM, FH, JMV, JH, AL,
841 JP

842 **Resources:** MCF, CAC, SS, SG, MV, YC, JP, TB, TSH, VP, ALC, AC, FH, MTI-Z, WM,
843 DME, AA, JMV, JH, TJL

844 **Supervision:** CAC, MCF

845 **Funding Acquisition :** CAC, MCF

846 **Conceptualization :** CAC, MCF, AL

847

848

849

References

- Armstrong-James, D., Meintjes, G., and Brown, G.D. (2014). A neglected epidemic: fungal infections in HIV/AIDS. *Trends Microbiol.* 22, 120–127.
- Bankevich, A., Nurk, S., Antipov, D., Gurevich, A.A., Dvorkin, M., Kulikov, A.S., Lesin, V.M., Nikolenko, S.I., Pham, S., Prjibelski, A.D., et al. (2012). SPAdes: a new genome assembly algorithm and its applications to single-cell sequencing. *J. Comput. Biol. J. Comput. Mol. Cell Biol.* 19, 455–477.
- Beale, M.A., Sabiiti, W., Robertson, E.J., Fuentes-Cabrejo, K.M., O'Hanlon, S.J., Jarvis, J.N., Loyse, A., Meintjes, G., Harrison, T.S., May, R.C., et al. (2015). Genotypic Diversity Is Associated with Clinical Outcome and Phenotype in Cryptococcal Meningitis across Southern Africa. *PLoS Negl. Trop. Dis.* 9, e0003847.
- Bicanic, T., Harrison, T., Niepieklo, A., Dyakopu, N., and Meintjes, G. (2006). Symptomatic Relapse of HIV-Associated Cryptococcal Meningitis after Initial Fluconazole Monotherapy: The Role of Fluconazole Resistance and Immune Reconstitution. *Clin. Infect. Dis.* 43, 1069–1070.
- Bicanic, T., Meintjes, G., Wood, R., Hayes, M., Rebe, K., Bekker, L.-G., and Harrison, T. (2007). Fungal burden, early fungicidal activity, and outcome in cryptococcal meningitis in antiretroviral-naïve or antiretroviral-experienced patients treated with amphotericin B or fluconazole. *Clin. Infect. Dis. Off. Publ. Infect. Dis. Soc. Am.* 45, 76–80.
- Bicanic, T., Wood, R., Meintjes, G., Rebe, K., Brouwer, A., Loyse, A., Bekker, L.-G., Jaffar, S., and Harrison, T. (2008). High-dose amphotericin B with flucytosine for the treatment of cryptococcal meningitis in HIV-infected patients: a randomized trial. *Clin. Infect. Dis. Off. Publ. Infect. Dis. Soc. Am.* 47, 123–130.
- Bovers, M., Hagen, F., Kuramae, E.E., and Boekhout, T. (2008). Six monophyletic lineages identified within *Cryptococcus neoformans* and *Cryptococcus gattii* by multi-locus sequence typing. *Fungal Genet. Biol. FG B* 45, 400–421.
- Brouwer, A.E., Rajanuwong, A., Chierakul, W., Griffin, G.E., Larsen, R.A., White, N.J., and Harrison, T.S. (2004). Combination antifungal therapies for HIV-associated cryptococcal meningitis: a randomised trial. *Lancet Lond. Engl.* 363, 1764–1767.
- Bui, T., Lin, X., Malik, R., Heitman, J., and Carter, D. (2008). Isolates of *Cryptococcus neoformans* from infected animals reveal genetic exchange in unisexual, alpha mating type populations. *Eukaryot. Cell* 7, 1771–1780.
- Capella-Gutiérrez, S., Silla-Martínez, J.M., and Gabaldón, T. (2009). trimAl: a tool for automated alignment trimming in large-scale phylogenetic analyses. *Bioinforma. Oxf. Engl.* 25, 1972–1973.
- Casadevall, A., and Perfect, J.R. (1998). *Cryptococcus neoformans* (Washington, D.C.: ASM Press).
- Chen, Y., Litvintseva, A.P., Frazzitta, A.E., Haverkamp, M.R., Wang, L., Fang, C., Muthoga, C., Mitchell, T.G., and Perfect, J.R. (2015). Comparative analyses of clinical and environmental populations of *Cryptococcus neoformans* in Botswana. *Mol. Ecol.* 24, 3559–3571.

- Chen, Y., Farrer, R.A., Giamberardino, C., Sakthikumar, S., Jones, A., Yang, T., Tenor, J.L., Wagih, O., Wyk, M.V., Govender, N.P., et al. (2017). Microevolution of Serial Clinical Isolates of *Cryptococcus neoformans* var. *grubii* and *C. gattii*. *mBio* 8, e00166-17.
- Cogliati, M. (2013). Global Molecular Epidemiology of *Cryptococcus neoformans* and *Cryptococcus gattii*: An Atlas of the Molecular Types. *Scientifica* 2013, 675213.
- Danecek, P., Auton, A., Abecasis, G., Albers, C.A., Banks, E., DePristo, M.A., Handsaker, R.E., Lunter, G., Marth, G.T., Sherry, S.T., et al. (2011). The variant call format and VCFtools. *Bioinformatics* 27, 2156–2158.
- Day, J.N. (2004). Cryptococcal Meningitis. *Pract. Neurol.* 4, 274–285.
- Desjardins, C.A., Giamberardino, C., Sykes, S.M., Yu, C.-H., Tenor, J.L., Chen, Y., Yang, T., Jones, A.M., Sun, S., Haverkamp, M.R., et al. (2017). Population genomics and the evolution of virulence in the fungal pathogen *Cryptococcus neoformans*. *Genome Res.*
- Desnos-Ollivier, M., Patel, S., Raoux-Barbot, D., Heitman, J., Dromer, F., and French Cryptococcosis Study Group (2015). Cryptococcosis Serotypes Impact Outcome and Provide Evidence of *Cryptococcus neoformans* Speciation. *mBio* 6, e00311.
- Dettman, J.R., Jacobson, D.J., and Taylor, J.W. (2003). A multilocus genealogical approach to phylogenetic species recognition in the model eukaryote *Neurospora*. *Evol. Int. J. Org. Evol.* 57, 2703–2720.
- Dromer, F., Mathoulin-Pélissier, S., Launay, O., Lortholary, O., and French Cryptococcosis Study Group (2007). Determinants of disease presentation and outcome during cryptococcosis: the CryptoA/D study. *PLoS Med.* 4, e21.
- Edgar, R.C. (2004). MUSCLE: multiple sequence alignment with high accuracy and high throughput. *Nucleic Acids Res* 32, 1792–1797.
- Engelthaler, D.M., Hicks, N.D., Gillece, J.D., Roe, C.C., Schupp, J.M., Driebe, E.M., Gilgado, F., Carriconde, F., Trilles, L., Firacative, C., et al. (2014). *Cryptococcus gattii* in North American Pacific Northwest: Whole-Population Genome Analysis Provides Insights into Species Evolution and Dispersal. *mBio* 5, e01464-14.
- Esher, S.K., Ost, K.S., Kozubowski, L., Yang, D.-H., Kim, M.S., Bahn, Y.-S., Alspaugh, J.A., and Nichols, C.B. (2016). Relative Contributions of Prenylation and Postprenylation Processing in *Cryptococcus neoformans* Pathogenesis. *mSphere* 1.
- Farrer, R.A., Desjardins, C.A., Sakthikumar, S., Gujja, S., Saif, S., Zeng, Q., Chen, Y., Voelz, K., Heitman, J., May, R.C., et al. (2015). Genome Evolution and Innovation across the Four Major Lineages of *Cryptococcus gattii*. *mBio* 6, e00868-815.
- Ferreira-Paim, K., Andrade-Silva, L., Fonseca, F.M., Ferreira, T.B., Mora, D.J., Andrade-Silva, J., Khan, A., Dao, A., Reis, E.C., Almeida, M.T.G., et al. (2017). MLST-Based Population Genetic Analysis in a Global Context Reveals Clonality amongst *Cryptococcus neoformans* var. *grubii* VNI Isolates from HIV Patients in Southeastern Brazil. *PLoS Negl. Trop. Dis.* 11, e0005223.
- Franzot, S.P., Salkin, I.F., and Casadevall, A. (1999). *Cryptococcus neoformans* var. *grubii*: separate varietal status for *Cryptococcus neoformans* serotype A isolates. *J. Clin. Microbiol.* 37, 838–840.

- Gerstein, A.C., Fu, M.S., Mukaremera, L., Li, Z., Ormerod, K.L., Fraser, J.A., Berman, J., and Nielsen, K. (2015). Polyploid titan cells produce haploid and aneuploid progeny to promote stress adaptation. *mBio* 6, e01340-1315.
- Gilbert, N.M., Donlin, M.J., Gerik, K.J., Specht, C.A., Djordjevic, J.T., Wilson, C.F., Sorrell, T.C., and Lodge, J.K. (2010). KRE genes are required for β -1,6-glucan synthesis, maintenance of capsule architecture and cell wall protein anchoring in *Cryptococcus neoformans*. *Mol. Microbiol.* 76, 517–534.
- Haas, B.J., Salzberg, S.L., Zhu, W., Pertea, M., Allen, J.E., Orvis, J., White, O., Buell, C.R., and Wortman, J.R. (2008). Automated eukaryotic gene structure annotation using EVIDENCEModeler and the Program to Assemble Spliced Alignments. *Genome Biol.* 9, R7.
- Hagen, F., Ceresini, P.C., Polacheck, I., Ma, H., van Nieuwerburgh, F., Gabaldón, T., Kagan, S., Pursall, E.R., Hoogveld, H.L., van Iersel, L.J.J., et al. (2013). Ancient dispersal of the human fungal pathogen *Cryptococcus gattii* from the Amazon rainforest. *PloS One* 8, e71148.
- Hagen, F., Khayhan, K., Theelen, B., Kolecka, A., Polacheck, I., Sionov, E., Falk, R., Parmen, S., Lumbsch, H.T., and Boekhout, T. (2015). Recognition of seven species in the *Cryptococcus gattii*/*Cryptococcus neoformans* species complex. *Fungal Genet. Biol. FG B.*
- Heitman, J., Kozel, T.R., Kwon-Chung, K.J., Perfect, J.R., and Casadevall, A. (2011). *Cryptococcus: From Human Pathogen to Model Yeast* (American Society of Microbiology).
- Hirakawa, M.P., Martinez, D.A., Sakthikumar, S., Anderson, M.Z., Berlin, A., Gujja, S., Zeng, Q., Zisson, E., Wang, J.M., Greenberg, J.M., et al. (2015). Genetic and phenotypic intra-species variation in *Candida albicans*. *Genome Res.* 25, 413–425.
- Hiremath, S.S., Chowdhary, A., Kowshik, T., Randhawa, H.S., Sun, S., and Xu, J. (2008). Long-distance dispersal and recombination in environmental populations of *Cryptococcus neoformans* var. *grubii* from India. *Microbiol. Read. Engl.* 154, 1513–1524.
- Hu, G., Liu, I., Sham, A., Stajich, J.E., Dietrich, F.S., and Kronstad, J.W. (2008). Comparative hybridization reveals extensive genome variation in the AIDS-associated pathogen *Cryptococcus neoformans*. *Genome Biol.* 9, R41.
- Hu, G., Wang, J., Choi, J., Jung, W.H., Liu, I., Litvintseva, A.P., Bicanic, T., Aurora, R., Mitchell, T.G., Perfect, J.R., et al. (2011). Variation in chromosome copy number influences the virulence of *Cryptococcus neoformans* and occurs in isolates from AIDS patients. *BMC Genomics* 12, 526.
- Hull, C.M., Davidson, R.C., and Heitman, J. (2002). Cell identity and sexual development in *Cryptococcus neoformans* are controlled by the mating-type-specific homeodomain protein Sxi1alpha. *Genes Dev.* 16, 3046–3060.
- Inglis, D.O., Skrzypek, M.S., Liaw, E., Muktali, V., Sherlock, G., and Stajich, J.E. (2014). Literature-Based Gene Curation and Proposed Genetic Nomenclature for *Cryptococcus*. *Eukaryot. Cell* 13, 878–883.
- Janbon, G., Ormerod, K.L., Paulet, D., Byrnes, E.J., Yadav, V., Chatterjee, G., Mullapudi, N., Hon, C.-C., Billmyre, R.B., Brunel, F., et al. (2014). Analysis of the genome and transcriptome of *Cryptococcus neoformans* var. *grubii* reveals complex RNA expression and microevolution leading to virulence attenuation. *PLoS Genet.* 10, e1004261.

- Jarvis, J.N., Meintjes, G., Rebe, K., Williams, G.N., Bicanic, T., Williams, A., Schutz, C., Bekker, L.-G., Wood, R., and Harrison, T.S. (2012). Adjunctive interferon- γ immunotherapy for the treatment of HIV-associated cryptococcal meningitis: a randomized controlled trial. *AIDS Lond. Engl.* *26*, 1105–1113.
- Jung, K.-W., Yang, D.-H., Maeng, S., Lee, K.-T., So, Y.-S., Hong, J., Choi, J., Byun, H.-J., Kim, H., Bang, S., et al. (2015). Systematic functional profiling of transcription factor networks in *Cryptococcus neoformans*. *Nat. Commun.* *6*.
- Kavanaugh, L.A., Fraser, J.A., and Dietrich, F.S. (2006). Recent Evolution of the Human Pathogen *Cryptococcus neoformans* by Intervarietal Transfer of a 14-Gene Fragment. *Mol. Biol. Evol.* *23*, 1879–1890.
- Khayhan, K., Hagen, F., Pan, W., Simwami, S., Fisher, M.C., Wahyuningsih, R., Chakrabarti, A., Chowdhary, A., Ikeda, R., Taj-Aldeen, S.J., et al. (2013). Geographically structured populations of *Cryptococcus neoformans* Variety *grubii* in Asia correlate with HIV status and show a clonal population structure. *PLoS One* *8*, e72222.
- Kwon-Chung, K.J. (1975). A new genus, *filobasidiella*, the perfect state of *Cryptococcus neoformans*. *Mycologia* *67*, 1197–1200.
- Kwon-Chung, K.J. (1976). A new species of *Filobasidiella*, the sexual state of *Cryptococcus neoformans* B and C serotypes. *Mycologia* *68*, 943–946.
- Kwon-Chung, K.J., Bennett, J.E., Wickes, B.L., Meyer, W., Cuomo, C.A., Wollenburg, K.R., Bicanic, T.A., Castañeda, E., Chang, Y.C., Chen, J., et al. (2017). The Case for Adopting the “Species Complex” Nomenclature for the Etiologic Agents of Cryptococcosis. *mSphere* *2*.
- Lawson, D.J., Hellenthal, G., Myers, S., and Falush, D. (2012). Inference of Population Structure using Dense Haplotype Data. *PLoS Genet* *8*, e1002453.
- Lee, D.-J., Bahn, Y.-S., Kim, H.-J., Chung, S.-Y., and Kang, H.A. (2015). Unraveling the novel structure and biosynthetic pathway of O-linked glycans in the Golgi apparatus of the human pathogenic yeast *Cryptococcus neoformans*. *J. Biol. Chem.* *290*, 1861–1873.
- Lengeler, K.B., Davidson, R.C., D’Souza, C., Harashima, T., Shen, W.C., Wang, P., Pan, X., Waugh, M., and Heitman, J. (2000a). Signal transduction cascades regulating fungal development and virulence. *Microbiol Mol Biol Rev* *64*, 746–785.
- Lengeler, K.B., Wang, P., Cox, G.M., Perfect, J.R., and Heitman, J. (2000b). Identification of the MATa mating-type locus of *Cryptococcus neoformans* reveals a serotype A MATa strain thought to have been extinct. *Proc. Natl. Acad. Sci. U. S. A.* *97*, 14455–14460.
- Lengeler, K.B., Cox, G.M., and Heitman, J. (2001). Serotype AD strains of *Cryptococcus neoformans* are diploid or aneuploid and are heterozygous at the mating-type locus. *Infect. Immun.* *69*, 115–122.
- Li, H. (2013). Aligning sequence reads, clone sequences and assembly contigs with BWA-MEM. *ArXiv13033997 Q-Bio*.
- Li, H., Handsaker, B., Wysoker, A., Fennell, T., Ruan, J., Homer, N., Marth, G., Abecasis, G., and Durbin, R. (2009). The Sequence Alignment/Map format and SAMtools. *Bioinformatics* *25*, 2078–2079.

- Li, L., Stoeckert, C.J., and Roos, D.S. (2003). OrthoMCL: identification of ortholog groups for eukaryotic genomes. *Genome Res* 13, 2178–2189.
- Lin, X., Hull, C.M., and Heitman, J. (2005). Sexual reproduction between partners of the same mating type in *Cryptococcus neoformans*. *Nature* 434, 1017–1021.
- Lin, X., Litvintseva, A.P., Nielsen, K., Patel, S., Floyd, A., Mitchell, T.G., and Heitman, J. (2007). α AD α Hybrids of *Cryptococcus neoformans*: Evidence of Same-Sex Mating in Nature and Hybrid Fitness. *PLOS Genet.* 3, e186.
- Lin, X., Patel, S., Litvintseva, A.P., Floyd, A., Mitchell, T.G., and Heitman, J. (2009). Diploids in the *Cryptococcus neoformans* Serotype A Population Homozygous for the α Mating Type Originate via Unisexual Mating. *PLoS Pathog* 5, e1000283.
- Litvintseva, A.P., and Mitchell, T.G. (2012). Population Genetic Analyses Reveal the African Origin and Strain Variation of *Cryptococcus neoformans* var. *grubii*. *PLoS Pathog* 8, e1002495.
- Litvintseva, A.P., Marra, R.E., Nielsen, K., Heitman, J., Vilgalys, R., and Mitchell, T.G. (2003). Evidence of sexual recombination among *Cryptococcus neoformans* serotype A isolates in sub-Saharan Africa. *Eukaryot. Cell* 2, 1162–1168.
- Litvintseva, A.P., Kestenbaum, L., Vilgalys, R., and Mitchell, T.G. (2005). Comparative Analysis of Environmental and Clinical Populations of *Cryptococcus neoformans*. *J. Clin. Microbiol.* 43, 556–564.
- Litvintseva, A.P., Thakur, R., Vilgalys, R., and Mitchell, T.G. (2006). Multilocus sequence typing reveals three genetic subpopulations of *Cryptococcus neoformans* var. *grubii* (serotype A), including a unique population in Botswana. *Genetics* 172, 2223–2238.
- Litvintseva, A.P., Lin, X., Templeton, I., Heitman, J., and Mitchell, T.G. (2007). Many Globally Isolated AD Hybrid Strains of *Cryptococcus neoformans* Originated in Africa. *PLOS Pathog.* 3, e114.
- Litvintseva, A.P., Carbone, I., Rossouw, J., Thakur, R., Govender, N.P., and Mitchell, T.G. (2011). Evidence that the human pathogenic fungus *Cryptococcus neoformans* var. *grubii* may have evolved in Africa. *PLoS One* 6, e19688.
- Liu, O.W., Chun, C.D., Chow, E.D., Chen, C., Madhani, H.D., and Noble, S.M. (2008). Systematic genetic analysis of virulence in the human fungal pathogen *Cryptococcus neoformans*. *Cell* 135, 174–188.
- Loftus, B.J., Fung, E., Roncaglia, P., Rowley, D., Amedeo, P., Bruno, D., Vamathevan, J., Miranda, M., Anderson, I.J., Fraser, J.A., et al. (2005). The genome of the basidiomycetous yeast and human pathogen *Cryptococcus neoformans*. *Science* 307, 1321–1324.
- Loyse, A., Wilson, D., Meintjes, G., Jarvis, J.N., Bicanic, T., Bishop, L., Rebe, K., Williams, A., Jaffar, S., Bekker, L.-G., et al. (2012). Comparison of the early fungicidal activity of high-dose fluconazole, voriconazole, and flucytosine as second-line drugs given in combination with amphotericin B for the treatment of HIV-associated cryptococcal meningitis. *Clin. Infect. Dis. Off. Publ. Infect. Dis. Soc. Am.* 54, 121–128.
- Lugarini, C., Goebel, C.S., Condas, L.A.Z., Muro, M.D., de Farias, M.R., Ferreira, F.M., and Vainstein, M.H. (2008). *Cryptococcus neoformans* Isolated from Passerine and Psittacine bird excreta in the state of Paraná, Brazil. *Mycopathologia* 166, 61–69.

Maccallum, I., Przybylski, D., Gnerre, S., Burton, J., Shlyakhter, I., Gnirke, A., Malek, J., McKernan, K., Ranade, S., Shea, T.P., et al. (2009). ALLPATHS 2: small genomes assembled accurately and with high continuity from short paired reads. *Genome Biol* 10, R103.

Maziarz, E.K., and Perfect, J.R. (2016). Cryptococcosis. *Infect. Dis. Clin. North Am.* 30, 179–206.

McKenna, A., Hanna, M., Banks, E., Sivachenko, A., Cibulskis, K., Kernytsky, A., Garimella, K., Altshuler, D., Gabriel, S., Daly, M., et al. (2010). The Genome Analysis Toolkit: a MapReduce framework for analyzing next-generation DNA sequencing data. *Genome Res* 20, 1297–1303.

Meyer, W., Marszewska, K., Amirmostofian, M., Igreja, R.P., Hardtke, C., Methling, K., Viviani, M.A., Chindamporn, A., Sukroongreung, S., John, M.A., et al. (1999). Molecular typing of global isolates of *Cryptococcus neoformans* var. *neoformans* by polymerase chain reaction fingerprinting and randomly amplified polymorphic DNA—a pilot study to standardize techniques on which to base a detailed epidemiological survey. *Electrophoresis* 20, 1790–1799.

Meyer, W., Aanensen, D.M., Boekhout, T., Cogliati, M., Diaz, M.R., Esposto, M.C., Fisher, M., Gilgado, F., Hagen, F., Kaocharoen, S., et al. (2009). Consensus multi-locus sequence typing scheme for *Cryptococcus neoformans* and *Cryptococcus gattii*. *Med. Mycol.* 47, 561–570.

Ngamskulrungrroj, P., Gilgado, F., Faganello, J., Litvintseva, A.P., Leal, A.L., Tsui, K.M., Mitchell, T.G., Vainstein, M.H., and Meyer, W. (2009). Genetic Diversity of the *Cryptococcus* Species Complex Suggests that *Cryptococcus gattii* Deserves to Have Varieties. *PLoS ONE* 4, e5862.

Ni, M., Feretzaki, M., Li, W., Floyd-Averette, A., Mieczkowski, P., Dietrich, F.S., and Heitman, J. (2013). Unisexual and Heterosexual Meiotic Reproduction Generate Aneuploidy and Phenotypic Diversity De Novo in the Yeast *Cryptococcus neoformans*. *PLOS Biol.* 11, e1001653.

Nielsen, K., Obaldia, A.L.D., and Heitman, J. (2007). *Cryptococcus neoformans* Mates on Pigeon Guano: Implications for the Realized Ecological Niche and Globalization. *Eukaryot. Cell* 6, 949–959.

Oliveira, M.T.B. de, Boekhout, T., Theelen, B., Hagen, F., Baroni, F.A., Lazera, M.S., Lengeler, K.B., Heitman, J., Rivera, I.N.G., and Paula, C.R. (2004). *Cryptococcus neoformans* Shows a Remarkable Genotypic Diversity in Brazil. *J. Clin. Microbiol.* 42, 1356–1359.

Ormerod, K.L., Morrow, C.A., Chow, E.W.L., Lee, I.R., Arras, S.D.M., Schirra, H.J., Cox, G.M., Fries, B.C., and Fraser, J.A. (2013). Comparative Genomics of Serial Isolates of *Cryptococcus neoformans* Reveals Gene Associated With Carbon Utilization and Virulence. *G3 Bethesda Md* 3, 675–686.

Park, B.J., Wannemuehler, K.A., Marston, B.J., Govender, N., Pappas, P.G., and Chiller, T.M. (2009). Estimation of the current global burden of cryptococcal meningitis among persons living with HIV/AIDS. *AIDS Lond. Engl.* 23, 525–530.

Patterson, N., Price, A.L., and Reich, D. (2006). Population structure and eigenanalysis. *PLoS Genet.* 2, e190.

- Pfeifer, B., Wittelsburger, U., Onsins, S.E.R., and Lercher, M.J. (2014). PopGenome: An efficient swiss army knife for population genomic analyses in R. *Mol. Biol. Evol.* msu136.
- Pritchard, J.K., Stephens, M., and Donnelly, P. (2000). Inference of population structure using multilocus genotype data. *Genetics* 155, 945–959.
- Rajasingham, R., Smith, S., Park, B., Jarvis, J., Govender, N., and Chiller, T. (2017). Global burden of disease if HIV-associated Cryptococcal meningitis: An updated analysis. *Lancet Infect. Dis.* 17, in press.
- Rhodes, J., Beale, M.A., Vanhove, M., Jarvis, J.N., Kannambath, S., Simpson, J.A., Ryan, A., Meintjes, G., Harrison, T.S., Fisher, M.C., et al. (2017). A Population Genomics Approach to Assessing the Genetic Basis of Within-Host Microevolution Underlying Recurrent Cryptococcal Meningitis Infection. *G3 Genes Genomes Genet.* 7, 1165–1176.
- Selvig, K., Ballou, E.R., Nichols, C.B., and Alspaugh, J.A. (2013). Restricted substrate specificity for the geranylgeranyltransferase-I enzyme in *Cryptococcus neoformans*: implications for virulence. *Eukaryot. Cell* 12, 1462–1471.
- Simwami, S.P., Khayhan, K., Henk, D.A., Aanensen, D.M., Boekhout, T., Hagen, F., Brouwer, A.E., Harrison, T.S., Donnelly, C.A., and Fisher, M.C. (2011). Low diversity *Cryptococcus neoformans* variety *grubii* multilocus sequence types from Thailand are consistent with an ancestral African origin. *PLoS Pathog.* 7, e1001343.
- Sionov, E., Lee, H., Chang, Y.C., and Kwon-Chung, K.J. (2010). *Cryptococcus neoformans* Overcomes Stress of Azole Drugs by Formation of Disomy in Specific Multiple Chromosomes. *PLoS Pathog* 6, e1000848.
- Stamatakis, A. (2014). RAxML version 8: a tool for phylogenetic analysis and post-analysis of large phylogenies. *Bioinformatics* 30, 1312–1313.
- Sun, S., Billmyre, R.B., Mieczkowski, P.A., and Heitman, J. (2014). Unisexual reproduction drives meiotic recombination and phenotypic and karyotypic plasticity in *Cryptococcus neoformans*. *PLoS Genet.* 10, e1004849.
- Taylor, J.W., Jacobson, D.J., Kroken, S., Kasuga, T., Geiser, D.M., Hibbett, D.S., and Fisher, M.C. (2000). Phylogenetic species recognition and species concepts in fungi. *Fungal Genet Biol* 31, 21–32.
- Ter-Hovhannisyan, V., Lomsadze, A., Chernoff, Y.O., and Borodovsky, M. (2008). Gene prediction in novel fungal genomes using an ab initio algorithm with unsupervised training. *Genome Res.* 18, 1979–1990.
- Vanhove, M., Beale, M.A., Rhodes, J., Chanda, D., Lakhi, S., Kwenda, G., Molloy, S., Karunaharan, N., Stone, N., Harrison, T.S., et al. (2017). Genomic epidemiology of *Cryptococcus* yeasts identifies adaptation to environmental niches underpinning infection across an African HIV/AIDS cohort. *Mol. Ecol.* 26, 1991–2005.
- Viviani, M.A., Esposito, M.C., Cogliati, M., Montagna, M.T., and Wickes, B.L. (2001). Isolation of a *Cryptococcus neoformans* serotype A MATa strain from the Italian environment. *Med. Mycol.* 39, 383–386.
- Vogan, A.A., and Xu, J. (2014). Evidence for genetic incompatibilities associated with post-zygotic reproductive isolation in the human fungal pathogen *Cryptococcus neoformans*. *Genome* 57, 335–344.

Wang, L., Zhai, B., and Lin, X. (2012). The link between morphotype transition and virulence in *Cryptococcus neoformans*. *PLoS Pathog.* 8, e1002765.

Xu, J., Vilgalys, R., and Mitchell, T.G. (2000). Multiple gene genealogies reveal recent dispersion and hybridization in the human pathogenic fungus *Cryptococcus neoformans*. *Mol. Ecol.* 9, 1471–1481.

Xue, C., Tada, Y., Dong, X., and Heitman, J. (2007). The human fungal pathogen *Cryptococcus* can complete its sexual cycle during a pathogenic association with plants. *Cell Host Microbe* 1, 263–273.

Yahara, K., Furuta, Y., Oshima, K., Yoshida, M., Azuma, T., Hattori, M., Uchiyama, I., and Kobayashi, I. (2013). Chromosome painting in silico in a bacterial species reveals fine population structure. *Mol. Biol. Evol.* 30, 1454–1464.

Yang, Z. (2007). PAML 4: phylogenetic analysis by maximum likelihood. *Mol. Biol. Evol.* 24, 1586–1591.

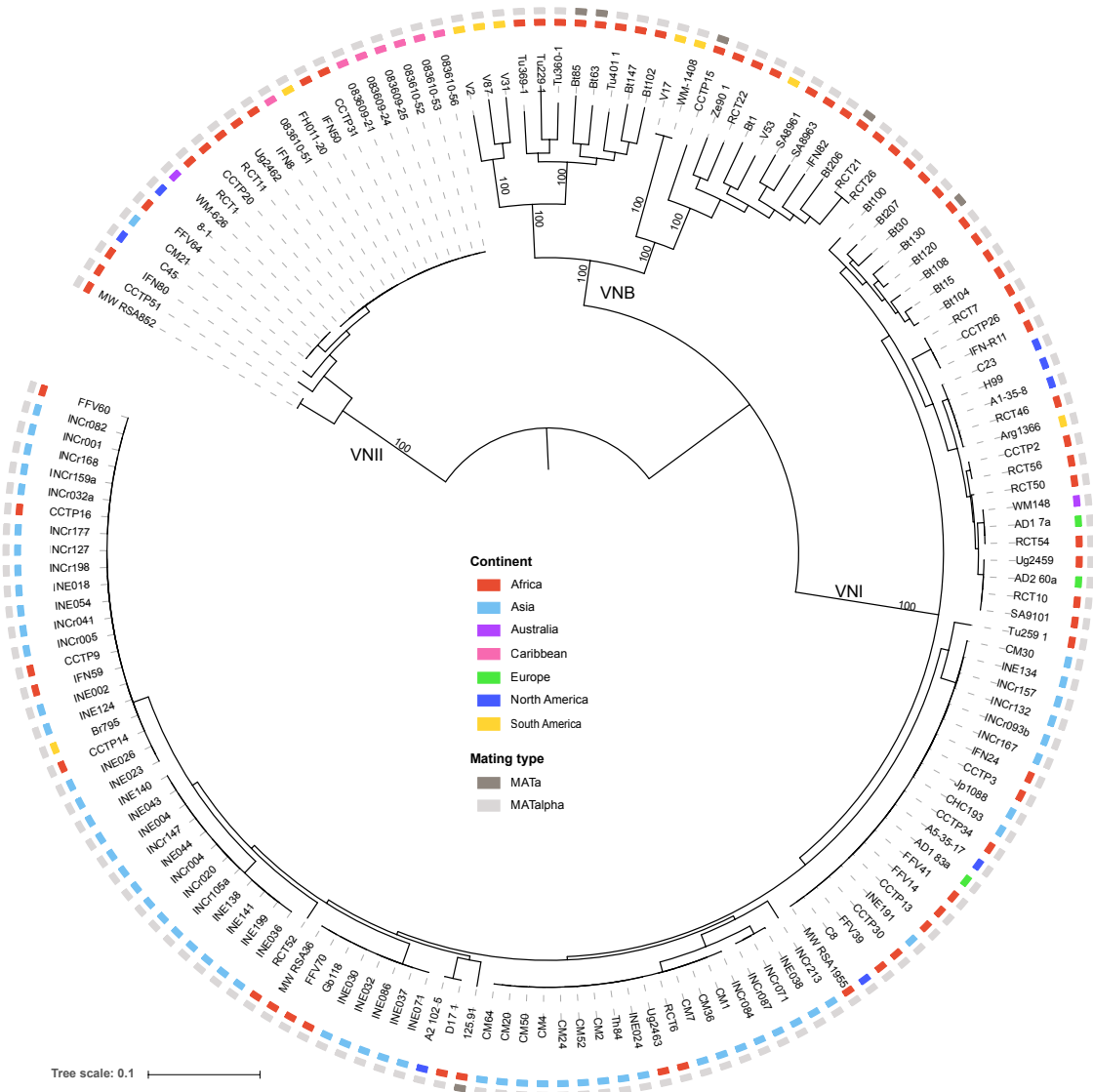


Figure 1. Phylogenetic analysis supports three major lineages of *C. neoformans* var. *grubii*. Using a set of 876,121 SNPs across the 159 non-hybrid isolates, a phylogenetic tree was inferred using RAxML. The tree was rooted with VNII as the outgroup (Hagen et al., 2015). The percentage of 1,000 bootstrap isolates that support each node is shown for major nodes with at least 90% support. For each isolate, the geographical site of isolation is noted by colored boxes.

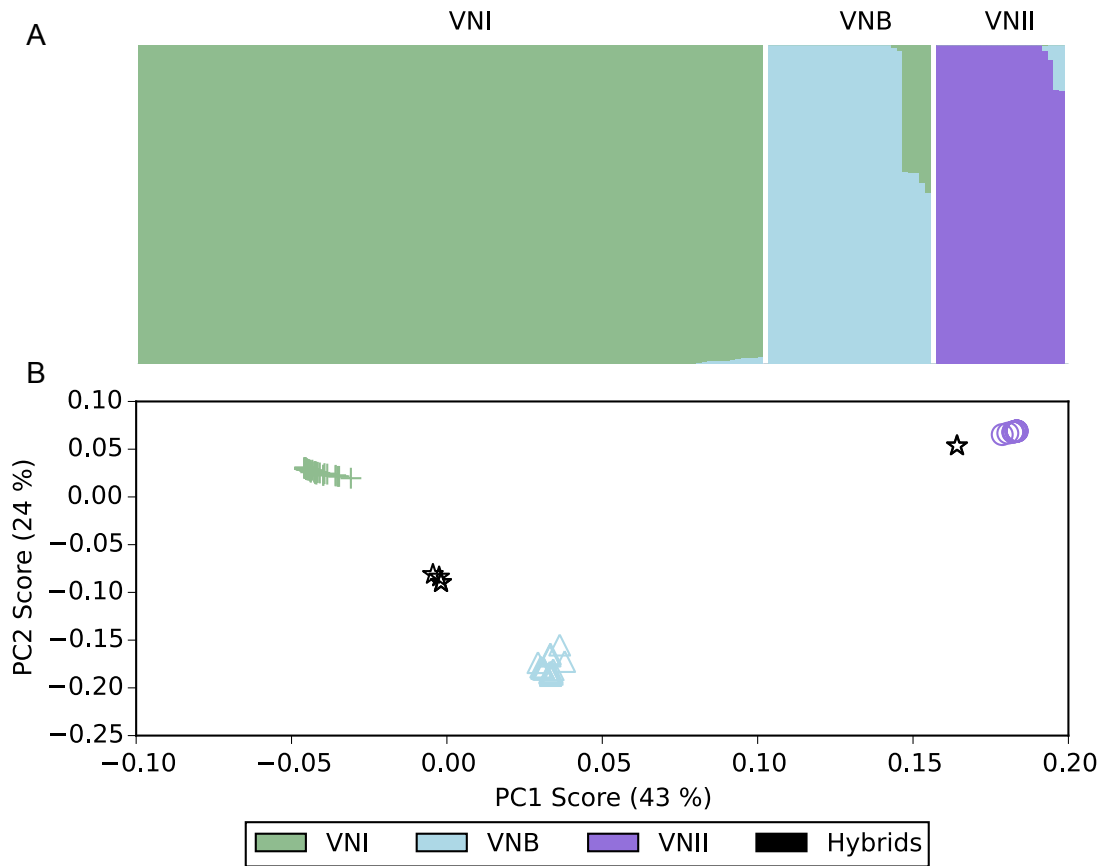


Figure 2. Ancestry characterization of three major groups highlights hybrid isolates. A. The fraction of ancestry (k=3) estimated by STRUCTURE is shown within a column for each isolate. B. Principal components analysis separates the 3 major lineages, with the hybrid isolates showing a mix of VNB ancestry with either VNI or VNII.

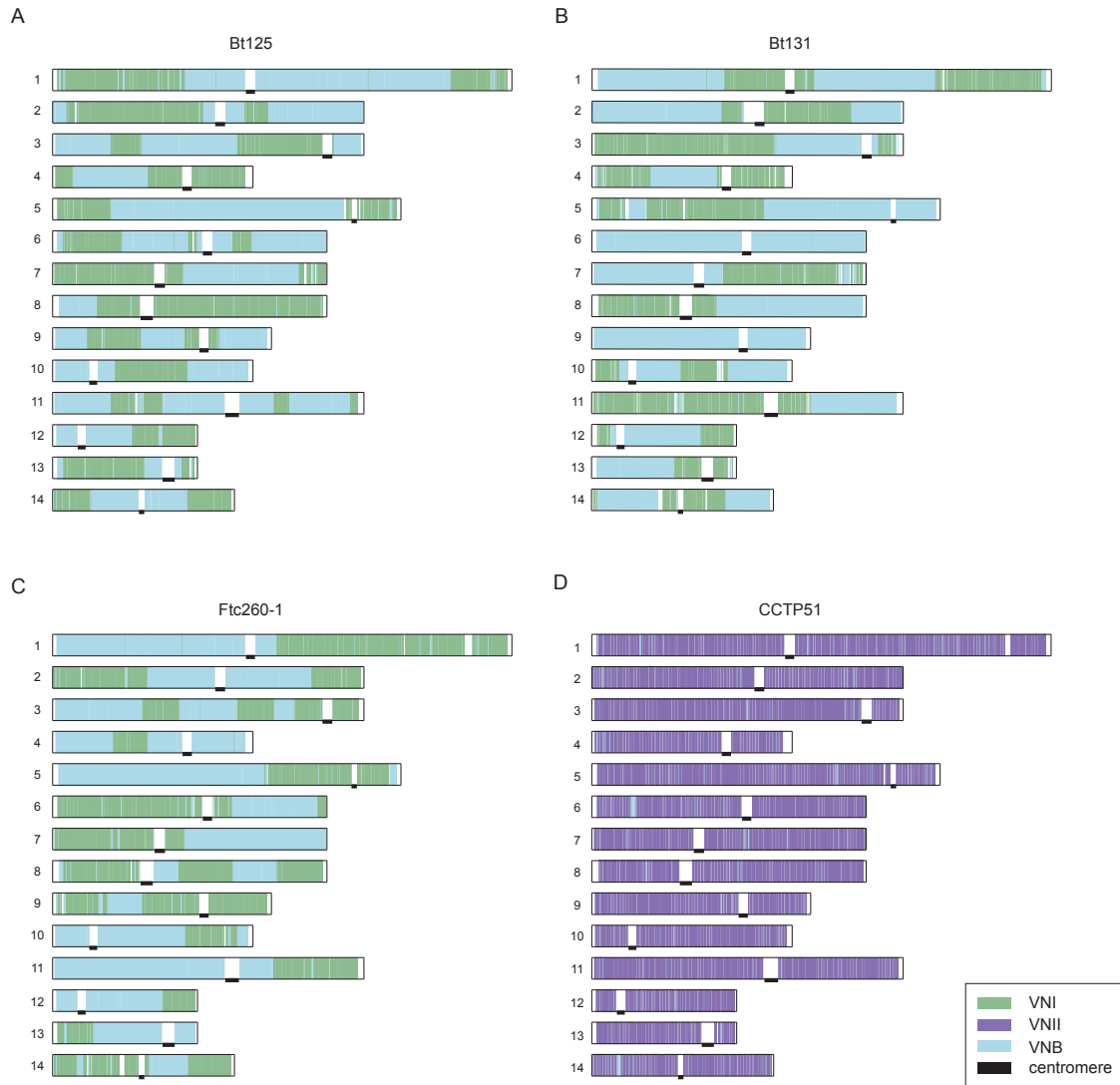


Figure 3. Large blocks of ancestry suggest recent recombination between lineages. For each of the four isolates depicted (A-D), the STRUSTRUCTURE assigned ancestry for each site along each chromosome is depicted as a colored bar corresponding to VNI, VNII, and VNB ancestry. Locations of centromeres are marked with black bars.

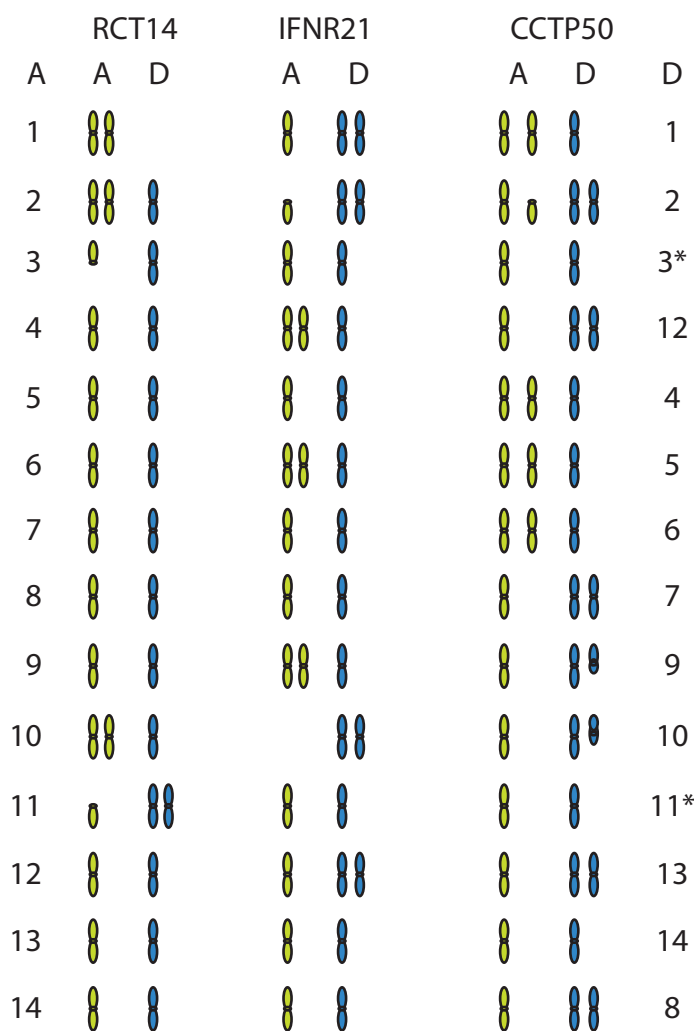


Figure 4. Chromosome ancestry and ploidy variation of AD hybrids. For three AD hybrid isolates (RCT14, IFNR21, and CCTP50), the contribution and copy number of A (green) and D (blue) ancestry chromosomal regions was measured by aligning all sequence reads to a combined AD reference (A:H99, left and D:JEC21, right). The copy number of each chromosome is depicted, with either full or partial chromosomal regions shown; see Figure S4 for detailed coverage plots for all AD hybrid isolates.

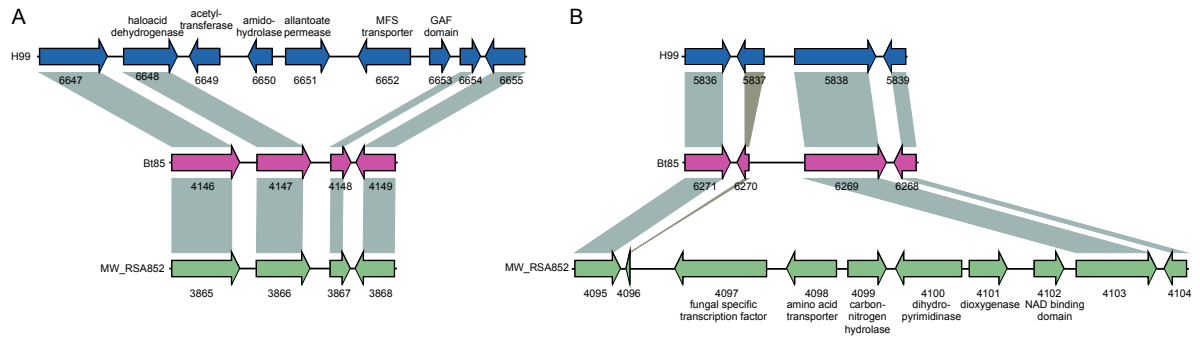


Figure 5. Lineage-specific gene clusters. Two large-lineage specific clusters were detected in the VNI genomes or VNII genomes; these are depicted using a representative genome from each lineage. A. Insertion of CNAG_06649 to CNAG_06653 in H99 (blue, VNI); syntenic genes in Bt85 (pink, VNB) and MW_RSA852 (green, VNII) are connected with grey bars. B. Insertion of C358_04097 to C358_04102 in MW_RSA852.

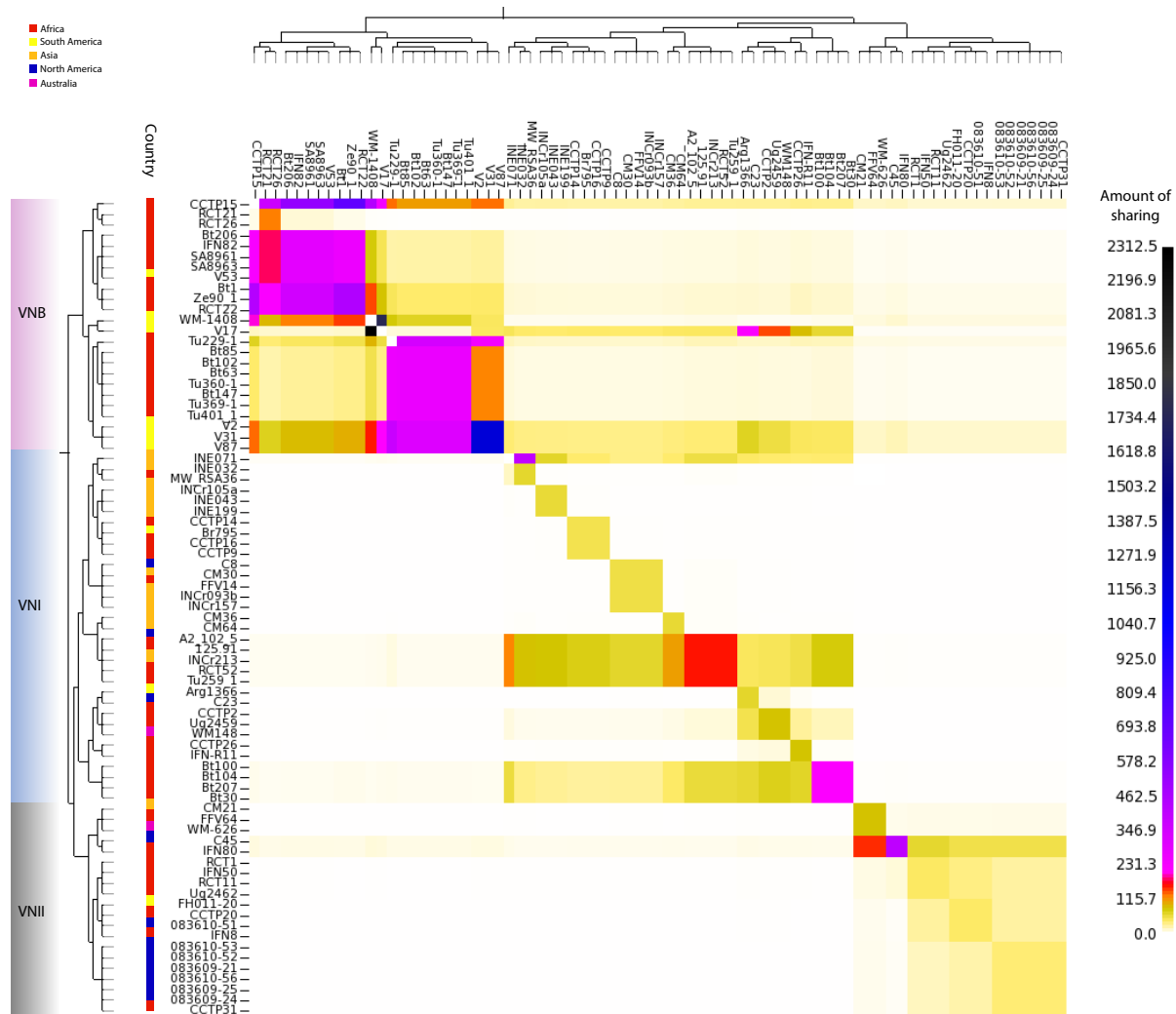


Figure 6. Genome-sharing analysis of *C. neoformans* var. *grubii* using fineStructure was performed on a SNP matrix using a representative of each clonal population within the VNI lineage. These genomes were reduced to a pairwise similarity matrix, which facilitates the identification of population structure based on haplotype sharing within regions of the genome. The x-axis represents the “donor” of genomic regions, while the y-axis represents the recipient of shared genomic regions. The scale bar represents the amount of genomic sharing, with black representing the largest amount of sharing of genetic material, and white representing the least amount of shared genetic material (no sharing). The geographical site of isolation is illustrated with coloured boxes as in Figure 1, and lineages are also shown.

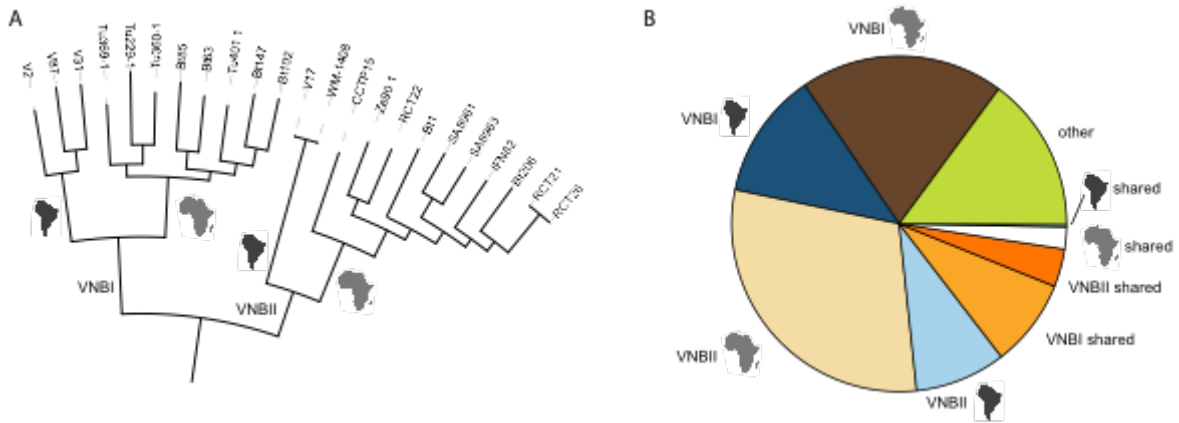


Figure 7. VNB alleles in population subdivisions and across geography. A. Phylogeny of VNB lineage showing major subdivisions (VNB-I and VNB-II) and inferred ancestral geography (South America or Africa, depicted as continent shapes). B. Classification of all 445,193 private VNB alleles (present in at least 1 VNB isolate and no VNI or VNII isolates) by subdivisions and geography. Most VNB alleles are specific for the each VNB subdivision and for the geographic subdivisions within each group. More alleles are shared between geographic locations in the same subdivision (VNB-I or VNB-II) than are shared within geographic locations across subdivisions.

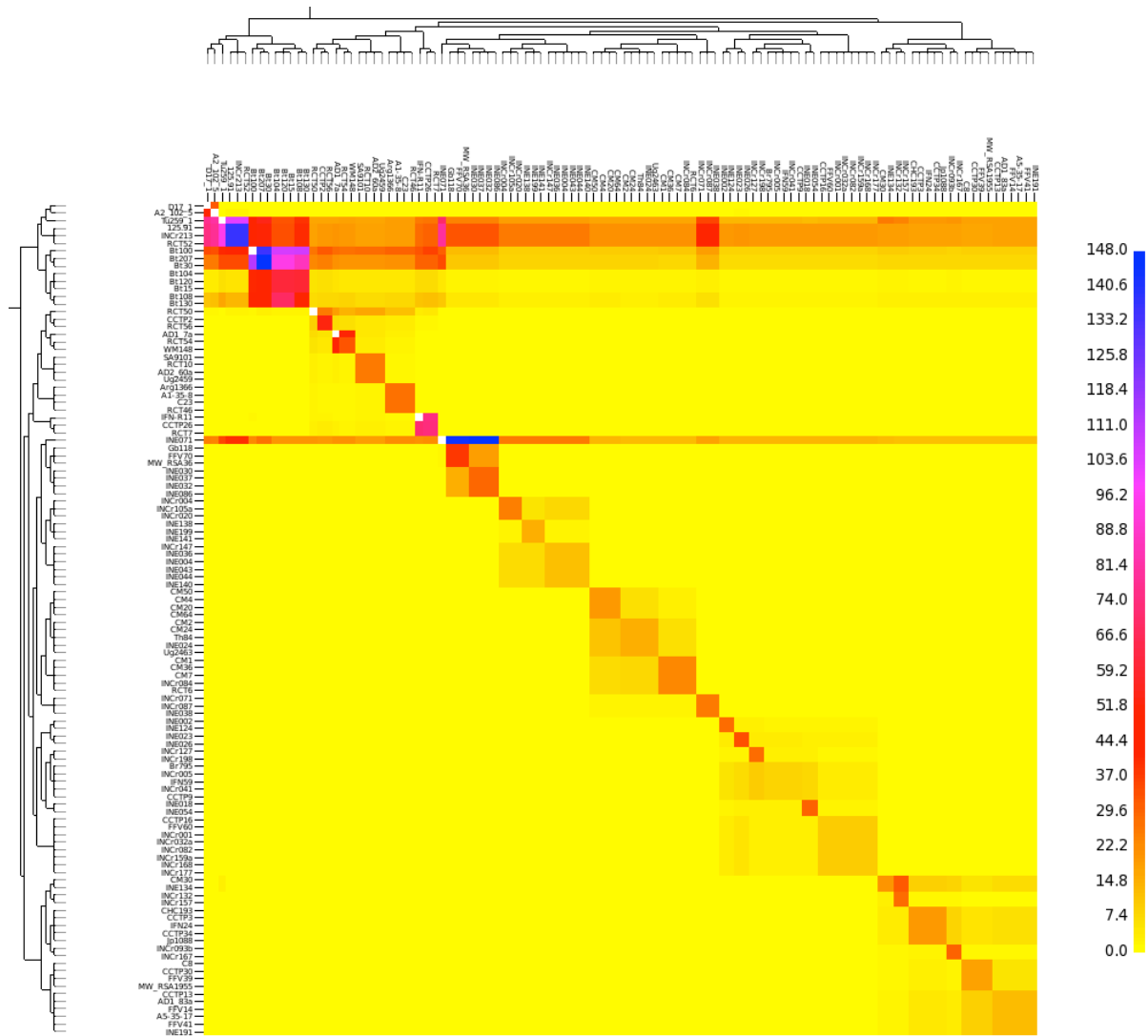


Figure 8. Genome-sharing analysis of the VNI lineage using fineStructure on a SNP matrix of 111 genomes. The x-axis represents the “donor” of genomic regions, whilst the y-axis represents the recipient of shared genomic regions. The scale bar represents the amount of genomic sharing, with blue representing the largest amount of sharing of genetic material, and yellow representing the least amount of shared genetic material (no sharing).

Table 1. Properties of sequenced isolates. For each population, the total number of isolates analyzed and the mating type(s) of the isolates are given.

Haploid isolates

Population	Isolates (#)	<i>MAT</i> α	<i>MATa</i>
VNI	111	109	2
VNII	23	23	0
VNB	25	21	4
VNI/VNB	5	1	4
VNII/VNB	2	2	0

Diploid isolates

Population	Isolates (#)	<i>MAT</i> α / <i>MAT</i> α	<i>MATa</i> / <i>MATa</i>	<i>MATa</i> / <i>MAT</i> α
VNI/VNB	1	1	0	0
VNII/VNB	2	2	0	0
VNB/Cnn*	8	0	1	7
VNB/Cg*	1	1	0	0

*Cnn: *C. neoformans* var. *neoformans*; Cg: *C. gattii*).

Table 2. Rapidly evolving genes in the three lineages of *C. neoformans* var. *grubii*. Consensus sequences were built for each lineage, and d_N and d_S were calculated for each lineage pair. As d_S was uniformly low throughout the dataset due to limited genetic diversity, for each pair of lineages we identified the 10 genes with assigned names (Inglis et al., 2014) with the highest d_N , which measures both the mutation rate and selection.

Comparison	d_N	Locus	Gene	Annotation
VNI vs VNB	0.0181	CNAG_01841	<i>GLN3</i>	transcription factor, deletion sensitive to organic peroxides (Jung et al., 2015)
	0.0155	CNAG_03894	<i>PDR802</i>	transcription factor, deletion with reduced virulence (Jung et al., 2015)
	0.0095	CNAG_03213	<i>UVE1</i>	UV damage endonuclease
	0.0092	CNAG_02756	<i>CDC43</i>	geranylgeranyltransferase-I, essential for virulence (Selvig et al., 2013)
	0.0090	CNAG_06655	<i>GPI18</i>	GPI-anchor transamidase
	0.0089	CNAG_01908	<i>HEM4</i>	uroporphyrinogen-III synthase
	0.0085	CNAG_03133	<i>ATG2602</i>	UDP-glucose sterol transferase
	0.0084	CNAG_03617	<i>CLP1</i>	clampless protein 1
	0.0076	CNAG_05740	<i>RAM1</i>	farnesyltransferase β -subunit, essential for virulence (Esher et al., 2016)
	0.0068	CNAG_03637	<i>YKU80</i>	Double strand break repair factor and silencing regulator, deletion has reduced virulence (Liu et al., 2008)
VNI vs VNII	0.0610	CNAG_05836	<i>HOC1</i>	α 1,6-mannosyltransferase (Lee et al., 2015)
	0.0408	CNAG_05838	<i>RGD1</i>	Rho GTPase activating protein, deletion has increased virulence (Liu et al., 2008)
	0.0214	CNAG_06031	<i>KRE63</i>	β -glucan synthase, involved in capsule and cell wall formation, deletion has decreased virulence (Gilbert et al., 2010)
	0.0149	CNAG_06814	<i>SXI1α</i>	α cell type transcription factor, required for mating (Hull et al., 2002)
	0.0142	CNAG_01841	<i>GLN3</i>	see above
	0.0135	CNAG_03229	<i>YOX101</i>	transcription factor, deletion sensitive to organic peroxides (Jung et al., 2015)
	0.0127	CNAG_03398	<i>ZIP2</i>	zinc ion transporter
	0.0113	CNAG_03133	<i>ATG2602</i>	see above
	0.0110	CNAG_03366	<i>ZNF2</i>	transcription factor, overexpression results in reduced virulence (Wang et al., 2012)
	0.0104	CNAG_01019	<i>SOD1</i>	superoxide dismutase
VNB vs VNII	0.0617	CNAG_05836	<i>HOC1</i>	see above
	0.0402	CNAG_05838	<i>RGD1</i>	see above
	0.0171	CNAG_06031	<i>KRE63</i>	see above
	0.0128	CNAG_03366	<i>ZNF2</i>	see above
	0.0122	CNAG_06814	<i>SXI1α</i>	see above
	0.0114	CNAG_03213	<i>UVE1</i>	see above
	0.0104	CNAG_01019	<i>SOD1</i>	see above
	0.0104	CNAG_03398	<i>ZIP2</i>	see above
	0.0102	CNAG_01841	<i>GLN3</i>	see above
	0.0102	CNAG_02756	<i>CDC43</i>	see above

Table 3. Population genetic features of the lineages of *C. neoformans* var. *grubii*. The total number of isolates, number of segregating sites, nucleotide diversity (π), and Tajima's D are given for each population.

Populations	Isolates (#)	Segregating sites	π	Tajima's D
VNI	111	190,716	0.00200	-0.107179
VNII	23	337,990	0.00105	-1.005950
VNB	25	613,991	0.00736	-0.232596

Table 4. Pairwise population genetic statistics between the lineages of *C. neoformans* var. *grubii*. The number of alleles fixed and shared between the populations, and alleles private to each population are given, along with divergence metrics dXY and F_{ST} .

Comparisons	Fixed	Shared	Private_A	Private_B	dXY	F_{ST}
VNB vs VNI	54,719	52,536	446,566	102,817	IvB: 0.0119	IvB: 0.595
VNB vs VNII	118,329	68,211	405,406	78,444	BvII: 0.0154	BvII: 0.707
VNI vs VNII	188,590	38,501	116,845	83,802	IvII: 0.0152	IvII: 0.874